THE UNIVERSITY *of* EDINBURGH

Nucleolar dynamics in cellular senescence

Gyuryang Park

S1570641

Principle Investigator: Dr. Tamir Chandra

Thesis submitted for the degree of Master of Science by Research in Genetics and Molecular Medicine

The University of Edinburgh

2021

Declaration

I hereby declare that the thesis has been composed entirely by myself and the results are solely my own work with the exception of following:

- RNA sequencing data was generated by the research group of Dr. Peter. D Adams
- RNA sequencing raw data was processed by Neil Robertson from the research group of Dr. Tamir Chandra

The thiesis has not been submitted for any other degree or professional qualification.

Signature: ..... Date: 26.02.21

Acknowledgements

First and foremost, I would like to express my deepest gratitude to Dr. Tamir Chandra who has responsibly supervised me and has been encouraging me throughout the period of my degree. Moreover, I am greatly grateful to Prof. Nick Gilbert who has been very supportive and helpful from the start to the end of the project. Secondly, I would like to show my wholehearted gratitude to Lizzie Freyer and Laura Murphy who have provided me great experimental or data analysis support and advice whenever needed. Besides, I cannot also stress enough brilliant imaging support from Harris Morrison, Matt Pearson, and Ann Wheeler. Last but not least, I would like to thank the colleagues from Dr. Tamir Chandra's research group who kindly offer me computational advice.

Abstract

The nucleolus is a subnuclear structure widely known as the site of ribosome biogenesis. Recently, additional functions of the nucleolus have been described, one of which is serving as a stress sensor. When the nucleolus senses stressors, it causes nucleolar stress characterised by changes to nucleolar area and function, along with signalling pathways including p53. Although alterations in nucleolar area were identified under nucleolar stress, the dynamic of nucleolar area triggered by different senescence inducers remains elusive. Besides, gene expression associated with enlarged nucleoli is not well understood. Here, I show nucleolar dynamics in different types of cellular senescence including oncogene-induced senescence (OIS), secondary senescence, and replicative senescence (RS). I have used human diploid fibroblast that were subjected to immunofluorescence with fibrillarin antibodies, which were subsequently quantitated by automated image analysis. I found enlarged nucleolar area upon the induction of OIS and RS but were not found in secondary senescence. Furthermore, nucleolar expansion was more significant in OIS than RS. In addition to nucleolar hypertrophy, changes in nuclear area and the enrichment of senescence-associated heterochromatin foci (SAHF) formation were identified along with enlarged nucleoli in OIS. Notably, SAHF-positive cells exhibited significantly enlarged nucleoli over SAHF-negative cells, suggesting alterations in nucleolar area may link with SAHF formation. Conversely, secondary senescence did not give rise to such nuclear alteration and chromosomal rearrangements. RS showed increased nuclear area, but no enrichment of SAHF formation in conjunction with nucleolar enlargement. The examination of candidate genes related with alterations in nucleoli in OIS and RS revealed distinct gene expression. For example, ribosomal protein L5 and L11 were overexpressed in OIS, yet they were suppressed in RS. The results demonstrate nucleolar stress in response to different senescence inducers leads to unique nucleolar dynamics, changes to nuclear and heterochromatin structure, and altered gene expression.

Lay Summary

The cell nucleus is where our genetic information is stored in the form of DNA within cells. The nucleolus is a subcompartment within the cell nucleus. Although it is traditionally recognised as a region to synthesise ribosomes, ancient evolutionary machines involved in the process of making proteins, other functions of the nucleoli have been recently uncovered, one of which is acting as a stress sensor. By sensing various stressors, internal or external stimuli which disrupt the stable state of cells, it can lead to alterations in nucleolar size. Additionally, nucleolar size has been proposed to play a role in ageing because having smaller nucleoli has been linked to an increased lifespan in worms, flies, and mice. However, we do not understand how nucleoli change upon cellular senescence, a system scientists study to understand human cellular ageing and cellular stress. Furthermore, gene activation linked with changes in nucleolar size is largely unknown. Therefore, the aim of the project is to investigate nucleolar dynamics in response to different senescence inducers and to examine the gene activation associated with increased nucleolar area.

Table of Contents

Declaration **2**

Acknowledgements **3**

Abstract **4**

Lay Summary **5**

Table of Contents **6**

List of Figures **9**

List of Tables **11**

Abbreviations **12**

Chapter I **14**

Introduction **14**

1: Introduction **14**

1.1: Nucleolus **14**

1.1.1: Ribosome biogenesis 15

1.1.2: Multiple functions of the nucleolus 16

1.1.3: Alterations by nucleolar stress 17

1.2: Diverse cellular response by nucleolar stress **19**

1.3: Cellular senescence **19**

1.3.1: Replicative senescence 20

1.3.2: Oncogene-induced senescence 22

1.3.3: Secondary senescence 22

1.4: Nucleolus and ageing **23**

Aims and Objectives **24**

Chapter II **26**

Materials and Methods **26**

2.1: Cell culture **26**

2.2: Cell proliferation assay **28**

2.3: Nucleoli staining **31**

2.4: Image acquisition **33**

2.5: Image sorting and quantification **34**

2.6: RNA sequencing and RNA sequencing analysis **36**

2.7: Statistical analysis **37**

Chapter III **38**

Results **38**

Nucleolar Dynamics in Oncogene-Induced Senescence **38**

3.1: Oncogene-induced senescence was caused by 4-OHT **38**

3.2: Examination of nucleolar area in oncogene-induced senescence **40**

3.2.1: Nucleolar area quantitated by CellProfiler 40

3.2.2: Nucleolar area quantitated by ImageJ 41

3.2.3: Nucleolar area was significantly increased by oncogene-induced senescence 44

3.3: Investigation of intracellular changes in oncogene-induced senescence **49**

3.3.1: Nuclear area was significantly increased by oncogene-induced senescence 49

3.3.2: Association between nucleolar hypertrophy and SAHF formation in oncogene-induced senescence 51

3.3.2.1: Introduction 51

3.3.2.2: Nucleolar hypertrophy may associate with SAHF formation 53

3.4: Examination of gene expression associated with alterations in nucleoli during oncogene-induced senescence **57**

3.4.1: Introduction 57

3.4.2: Ribosomal protein genes and RRN3 were upregulated, yet JAZF1, nucleolar protein genes and lamin protein genes were downregulated in oncogene-induced senescence 59

Chapter IV **61**

Nucleolar Dynamics in Secondary Senescence **61**

4.1: Secondary senescence was triggered by cell-cell interaction **61**

4.2: Investigation of nucleolar area in secondary senescence **62**

4.2.1: Nucleolar hypertrophy was not identified in secondary senescence 62

4.3: Examination of intracellular changes in secondary senescence **68**

4.3.1: Secondary senescence did not cause changes in nuclear area and SAHF formation 68

Chapter V 71

Nucleolar Dynamics in Replicative Senescence 71

5.1: Long-term serial passage induced replicative senescence 71

5.2: Inspection of nucleolar area in replicative senescence 74

5.2.1: Optimisation of antibody concentration for immunofluorescence 74

5.2.2: Nucleolar area was significantly increased by replicative senescence 75

5.3: Investigation of intracellular changes in replicative senescence 82

5.3.1: Nuclear area was significantly increased, yet there was no enrichment of SAHF in replicative senescence 82

5.4: Examination of gene expression linked with alterations in nucleoli during replicative senescence 84

5.4.1: RPL15, RRN3, and JAZF1 were overexpressed, yet nucleolar protein genes, lamin protein genes, RPL5, RPL11, and SUN1 were repressed in replicative senescence 84

Chapter VI 86

Discussion 86

6.1: Nucleolar expansion under nucleolar stress and diseases 86

6.2: Nucleolar expansion alongside alterations in nuclear size and SAHF formation 89

6.3: Genes expressed alongside alterations in nucleolar area 90

References 93

List of Figures

Figure 1: A schematic diagram of nucleus, nucleolus, and nucleolar sub-compartments 15

Figure 2: The process of ribosome generation in mammalian cells .. 16

Figure 3: A simplified schematic diagram of intracellular events under normal conditions and nucleolar stress 18

Figure 4: Co-culture system used for the induction of oncogene-induced and secondary senescence 27

Figure 5: EdU incorporation assay of ER:Ras IMR90 39

Figure 6: Nucleolar and nuclear area measured by CellProfiler 40

Figure 7: Nucleolar area measurement by ImageJ 42

Figure 8: Correlation coefficient between CellProfiler and ImageJ 43

Figure 9: Nucleolar area was significantly enlarged in day 7 ER:Ras IMR90 44

Figure 10: Immunofluorescence images of co-cultured ER:Ras IMR90 and mVenus:EV 46

Figure 11: Investigation of nucleolar area at different time point during OIS 46

Figure 12: Nucleolar area examination in the time course of OIS 47

Figure 13: Inspection of nucleolar area between control and day 7 and between day 7 EdU-positive and day 7 EdU-negatvie ER:Ras IMR90 49

Figure 14: Nuclear area became significantly greater during OIS 50

Figure 15: A significant increase in nuclear area was caused by OIS 51

Figure 16: Images of SAHF-negative and –positive ER:Ras IMR90 . 52

Figure 17: Nucleolar area comparison between day 7 SAHF-negative and day 7 SAHF-positive cells in OIS 53

Figure 18: Nucleolar size comparison between day 7 SAHF-negative and day 7 SAHF-positive ER:Ras IMR90 54

Figure 19: A schematic diagram of immunofluorescently-stained and EdU-stained ER:Ras IMR90 cells 56

Figure 20: Nucleolar expansion seems to associate with SAHF formation in OIS 56

Figure 21: RNA-seq analysis of genes linked with nucleolar alterations in OIS 60

Figure 22: Secondary senescence was determined by EdU assay .. 62

Figure 23: The measurement of nucleoli in mVenus:EV using CellProfiler and ImageJ 63

Figure 24: Nucleolar area was not significantly altered in day 7 mVenus:EV 63

Figure 25: The examination of nucleolar area in the course of secondary senescence 64

Figure 26: Nucleolar size was not altered throughout the time-course experiment 65

Figure 27: Secondary senescence did not trigger changes in nucleolar size whereas OIS induced nucleolar hypertrophy 67

Figure 28: Nuclear area was not significantly changed by secondary senescence 68

Figure 29: The examination of nuclear size in the course of secondary senescence 69

Figure 30: Prolonged culture of IMR90 human fibroblasts induced RS 72

Figure 31: EdU incorporation assay of IMR90 human fibroblasts 73

Figure 32: Antibody dose optimisation for immunofluorescence 74

Figure 33: Immunofluorescence staining of IMR90 human fibroblasts and nucleolar size quantification by CellProfiler 76

Figure 34: The examination of nucleolar area and the number of nucleolus per nucleus in RS 78

Figure 35: Immunofluorescence assay of IMR90 human fibroblasts and nucleolar area quantification by CellProfiler 79

Figure 36: Nucleolar enlargement was induced by RS 80

Figure 37: The comparison of nucleolar area between early and late passage cells and between EdU-positive and EdU-negative cells 81

Figure 38: Nucleolar expansion was found to be more severe in OIS than RS 82

Figure 39: Significantly increased nuclear area was identified in late-passage IMR90 human fibroblasts compared to early-passage fibroblasts 83

Figure 40: RNA-seq analysis of genes associated with nucleolar alterations in RS 85

List of Tables

Table 1: An alternative reaction mix prepared for EdU incorporation assay 29

Table 2: The total number of cells and culture period recorded during long term serial passage of IMR90 cells 29

Table 3: The number of cells seeded in one cell culture dish and the number of proliferated cells identified prior to passaging 30

Table 4: The accumulated cell counts and total culture period during IMR90 serial passaging 31

Table 5: Dilution factor used for preparing antibody with different concentration 32

Table 6: Antibodies used for immunofluorescence 33

Table 7: Exposure values to acquire immunofluorescence images 34

Table 8: P-values in line with symbols used to determine statistical significance 37

Table 9: The list of genes associated with nucleolar area, structure, or morphology 58

Abbreviations

OIS	oncogene-induced senescence
RS	replicative senescence
SAHF	senescence-associated heterochromatin foci
NORs	nucleolus organising regions
rRNA	ribosomal RNA
rDNA	rRNA genes
FC	fibrillar centre
DFC	dense fibirillar component
GC	granular component
pre-rRNA	pre-ribosomal RNA
ITS	internal transcribed spacers
5′-ETS	5′ external transcribed spacers
3′-ETS	3′ external transcribed spacers
snoRNPs	small nucleolar ribonucleoproteins
snoRNAs	small nucleolar RNAs
UV	ultraviolet
NPs	nucleolar proteins
RPs	ribosomal proteins
MDM2	mouse double minute 2
GLTSCR2	glioma tumor suppressor candidate region gene 2
MYBBP1A	MYB binding protein 1A
BAX	Bcl-2-associated X
RPL5	ribosomal protein L5
RPL11	ribosomal protein L11
DDR	DNA damage response
SASP	senescence-associated secretary phenotype
TRF2	telomeric repeat-binding factor 2
POT1	protection of telomeres 1
ATR	ataxia telangiectasia and Rad3-related
ATM	ataxia-telangiectasia mutated
TERT	telomerase reverse transcriptase
NIS	Notch-induced senescence

SGS1	slow growth suppressor 1
HGPS	Hutchinson-Gilford progeria syndrome
4-OHT	4-hydroxytamoxifen
EdU	5-ethynyl-2′-deoxyuridine
UBF	upstream binding factor
DNMT1	DNA methyltransferase 1
HMGA	High-Mobility Group A
RNA-seq	RNA sequencing
FBL	fibrillarin
NCL	nucleolin
NOL11	nucleolar protein 11
NOL12	nucleolar protein 12
JAZF1	juxtaposed with another zinc finger protein 1
PD	Parkinson's disease
H_2O_2	hydrogen peroxide
aluRNAs	RNA polymerase II transcripts originating from intronic Alu elements
SAHDs	senescence-associated heterochromatin domains
FACS	fluorescence-associated cell sorter

Chapter I

Introduction

1: Introduction

1.1: Nucleolus

The nucleolus is a membrane-less organelle within the nuclei. It is one of the most visible intranuclear structures and this drew attention of many scientists in the twentieth century. In 1934, the formation of nucleoli were found to originate at specific chromosomal loci in *Zea Mays* by McClintock (McClintock, 1934), termed nucleolus organising regions (NORs). The NORs were later identified as a cluster of ribosomal RNA (rRNA) genes by DNA-isotopically labelled RNA hybridisation in *Drosophila melanogaster* and *Xenopus laevis* (Birnstiel et al., 1966; Ristossa and Spiegelman, 1965). A similar approach led to uncover human rRNA genes (rDNA) located on acrocentric chromosomes 13, 14, 15, 21, and 22 (Henderson et al., 1972). Today, it is known that rRNA genes are organised in tandem arrays and the nucleolus has three sub-compartments, the fibrillar centre (FC), dense fibirillar component (DFC), and granular component (GC), all of which can be observed under an electron microscopy (Boisvert et al., 2007; Hein et al., 2013) (Figure 1). These sub-regions of the nucleolus are involved in a traditionally well-known nucleolar function, ribosome biogenesis. Moreover, with advanced proteomic analysis, nucleolar functions have been expanded beyond being a ribosome factory, for example, orchestrating cellular stress response, cell cycle regulation, telomerase assembly, and ageing (Lee et al., 2014; Rubbi and Milner, 2003; Tiku et al., 2017; Yuan et al., 2005).

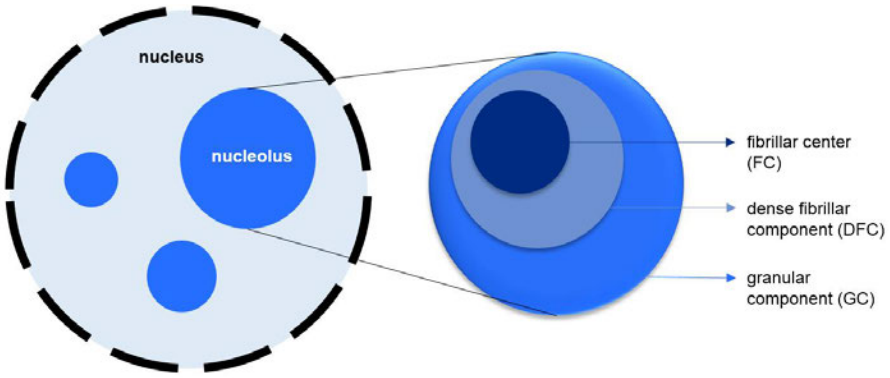

Figure 1: A schematic diagram of nucleus, nucleolus, and nucleolar sub-compartments: Nucleoli are present inside the nucleus and they have three structures - fibrillar center, dense fibrillar component, and granular component.

1.1.1: Ribosome biogenesis

The major function of the nucleolus is generating ribosomes that are indispensable for protein synthesis. Overall, ribosome biogenesis involves pre-ribosomal RNA (pre-rRNA) processing and maturation and ribosome assembly with ribosomal proteins (Figure 2) (Boisvert et al., 2007). rDNAs are transcribed by RNA polymerase I at the boundary of FC and DFC leading to 47S pre-rRNA production. The primary 47S rRNA transcript contains not only 18S, 5.8S, and 28S rRNA but also internal transcribed spacers (ITS) and it is flanked by 5′ and 3′ external transcribed spacers (5′-ETS and 3′-ETS respectively) (Henras et al., 2015). ITS, 5′-ETS, and 3′-ETS are subsequently eliminated by the association with pre-rRNA processing factors including small nucleolar ribonucleoproteins (snoRNPs) and small nucleolar RNAs (snoRNAs) whose genes are generally transcribed by RNA polymerase II and III in the nucleoplasm. As a consequence, mature 18S, 5.8S, and 28S rRNAs are generated. Unlike other rRNA genes, 5S rRNA genes are transcribed by RNA polymerase III. Following rRNA maturation, ribosomal small subunit 40S and large subunit 60S are made by the assembly of mature rRNAs with ribosomal proteins. The small and large subunits are independently transported to the cytoplasm in which mature 80S ribosomes are established and they are ready to translate

mRNAs into proteins (Boisvert et al., 2007; Hein et al., 2013; Henras et al., 2015).

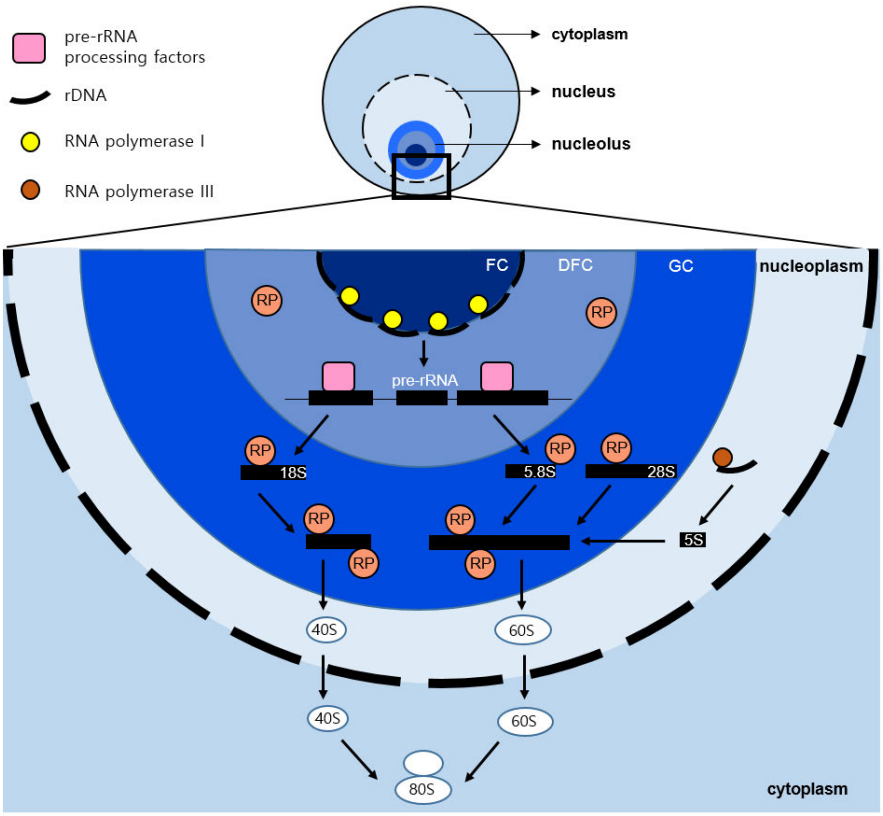

Figure 2: The process of ribosome generation in mammalian cells: The production of a functional ribosome requires several steps. Firstly, rDNA is transcribed by RNA polymerase I and that initially gives rise to pre-rRNA transcripts. The pre-rRNAs are subsequently processed, generating mature rRNAs. These mature rRNAs subsequently interact with ribosomal proteins, forming ribosomal small 40S and large 60S subunits. Finally, the small and large subunits are assembled together to create mature ribosome in the cytoplasm (Figure was modified from Boisvert et al., 2007).

1.1.2: Multiple functions of the nucleolus

The nucleolus was found to have a function other than ribosome biogenesis owing to the incorporation of Mass Spectrometry and bioinformatics into nucleolar proteomic analysis. Approximately 30 percent of nucleolar proteins were reported to have functions engaged in ribosome production, while the roles of other nucleolar proteins were

not determined (Ahmad et al., 2008; Anderson et al., 2002). Since then, there has been accumulating evidence that the nucleolus plays an important role in other cellular processes. For instance, the assembly of active telomerase was found to be in DFC (Lee et al., 2014). Another nucleolar function is cell cycle regulation: the depeletion of rDNA transcription factor, TIF-IA, led to cell cycle arrest and p53-dependent apoptosis (Yuan et al., 2005). Additionally, a number of studies suggested the size of the nucleolus is correlated with ageing across species (Buchwalter and Hetzer, 2017; Sinclair et al., 1997; Tiku et al., 2017), which will be later described. Interestingly, the nucleolus was discovered to act as a hub where diverse stress stimuli are sensed and coordinated (Rubbi and Milner, 2003). This leads to a new emerging concept, nucleolar stress. Nucleolar stress refers to a biological event characterised by a variety of alterations in nucleolar area and function along with changes to internal signalling pathways such as p53 when stressors are sensed by the nucleolus (Hein et al., 2013; Yang et al., 2018). The stressors include replicative stress, abnormal expression of oncogenes, reactive oxygen species, ultraviolet (UV), and chemo-therapeutic drugs (Al-Baker et al., 2004; Burger et al., 2010; Nishimura et al., 2015; Pinho et al., 2019; Wang et al., 2012).

1.1.3: Alterations by nucleolar stress

In normal physiological conditions, rRNAs are transcribed and ribosomes are generated as usual (Figure 3). Nucleolar proteins (NPs) and ribosomal proteins (RPs) may shuttle between the nucleolus and the nucleoplasm (the protoplasm of the nucleus) at basal level due to the absence of a membrane in the nucleolus. Importantly, cells keep maintaining the low level of tumour suppressor protein p53 by the association with mouse double minute 2 (MDM2; human homolog, HDM2) leading to p53 ubiquitination and subsequently its degradation (Rubbi and Milner, 2003). By contrast, under nucleolar stress, ribosome biogenesis is impaired and nucleolar area or morphology is distorted (Al-Baker et al., 2004; Burger et al., 2010; Chen et al., 2018; Nishimura et al., 2015; Pinho et al., 2019; Wang et al., 2012) (Figure

3). Moreover, p53 is no longer associated with MDM2 resulting in p53 stabilisation and activation. NPs and RPs play a key role by substantially translocating from the nucleolus to the nucleoplasm in response to stressors and suppressing the interaction between MDM2 and p53. For example, the translocation of NPs including nucleophosmin and glioma tumour suppressor candidate region gene 2 (GLTSCR2) bound to MDM2, which leads to p53 accumulation in the nucleoplasm (Chan et al., 1987; Kurki et al., 2004; Lee et al., 2012). Besides, translocated MYB binding protein 1A (MYBBP1A) contributed to p53 acetylation and that switched on its downstream target genes including p21 and Bcl-2-associated X (BAX) (Kumazawa et al., 2015). Likewise, RPs, such as ribosomal protein L5 and L11 (RPL5 and RPL11 respectively) moved to the nucleoplasm and inhibited MDM2 interaction with p53 (Dai and Lu, 2004; Zhang et al., 2003). Later, 5S rRNA was found to be essential to form ribonucleoproteins in concert with RPL11 and RPL5, which together regulates MDM2 (Donati et al., 2013; Li and Gu, 2011). Furthermore, nucleolar stress induced by actinomycin D and etoposide, which cause rDNA transcription inhibition and DNA double strand breaks respectively, confirms our understanding of the relocalisation of nucleolar proteins and the dynamic of the nucleolar proteome (Anderson et al., 2005; Boisvert et al., 2010). In summary, nucleolar stress results in the activation of p53 and the disruption of nucleolar area or morphology, ribosome biogenesis, and nucleolar proteome.

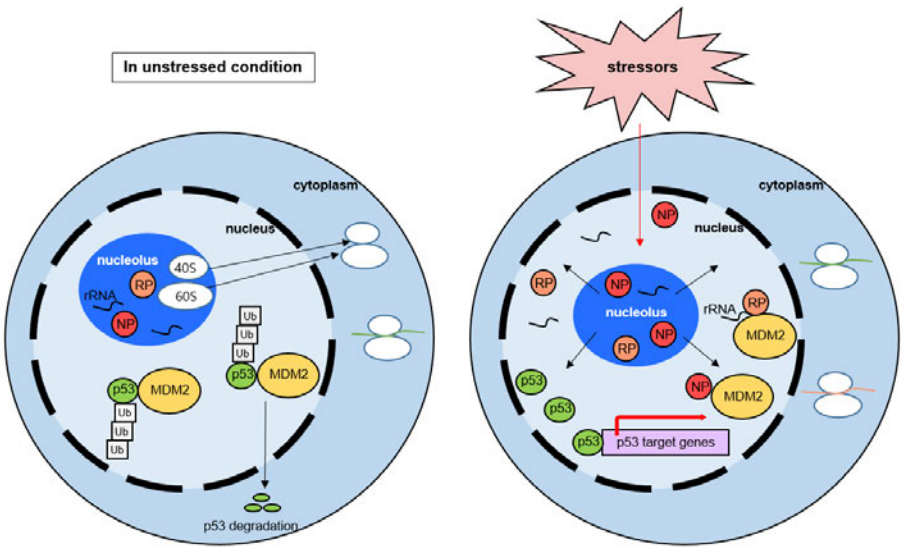

Figure 3: A simplified schematic diagram of intracellular events under normal conditions and nucleolar stress: In unstressed condition, ribosome biogenesis remains stable and RPs and NPs may travel between nucleolus and nucleoplasm at basal level. p53 proteins are prone to be degraded due to binding with MDM2 leading to p53 ubiquitination and degradation by proteasome. However, p53 is accumulated and becomes active under nucleolar stress partly because of relocated NPs and RPs to the nucleoplasm where they can associate with MDM2, thereby inhibiting MDM2-p53 interaction (Figure was modified from Hein et al., 2013).

1.2: Diverse cellular responses by nucleolar stress

Following nucleolar stress, cells differently react to the stressors and the cellular stress response can vary from recovery to cell death. In essence, the stressors cause DNA damage response (DDR) involved in DNA damage repair and it results in the cell cycle phase transition from G1 to G0 quiescent state (d'Adda di Fagagna, 2008). If DNA damage is properly repaired by DNA repair mechanisms, such as base or nucleotide excision repair or double-strand break repair, cells become committed to re-enter G1 phase and restart normal proliferation. However, when DNA damage is too severe for DDR to tackle, it stimulates apoptosis to eliminate damaged cells and it consequently leads to cell death. Alternatively, cells can enter a permanent G1 arrest, becoming senescent and preventing the proliferation of damaged cells (d'Adda di Fagagna, 2008). This irreversible cellular condition is known as cellular senescence. In the following chapter, cellular senescence will be introduced in depth.

1.3: Cellular senescence

Cellular senescence can be defined as the state of cells being alive and metabolically active but incapable of proliferation in response to various senescence inducers including a finite number of cell divisions, aberrant oncogene expression, or muted anti-oncogene expression (Campisi and d'Adda di Fagana, 2007; Kuilman et al., 2010; Pérez-Mancera et al., 2014). Distinct senescence inducers give rise to

different types of senescence including replicative, oncogene-induced, and secondary senescence. The noticeable characteristics of senescent cells are changed gene expression and chromatin reorganisation. For instance, the upregulation of tumour suppressor genes such as p53 and p16 were shown to be accompanied by senescence in H-ras V12-transduced human fibroblasts and mouse embryo fibroblasts (Serrano et al., 1997). Such changed gene expression in senescent cells affects the intercellular interactions in their cellular microenvironment via senescence-associated secretary phenotype (SASP). The SASP factors are senescence-associated secretomes from senescent cells that include proinflammatory cytokines, growth factors, chemokines, and proteases, which together have different roles in the physiology of organisms (Pérez-Mancera et al., 2014). Another feature of senescence is heterochromatin reorganisation called senescence-associated heterochromatin foci (SAHF) identified from oncogene-induced senescence (OIS) (Narita et al., 2003). Additionally, cells that established replicative senescence (RS) were found to exhibit morphological and biochemical changes such as enlarged nuclei and senescence-associated β-galactosidase activity (Dimri et al., 1995; Hayflick, 1965). All these cellular characteristics are believed to be the hallmarks of senescence. Yet, the features of senescent cells vary across the types of senescence and cells. One example can be SAHF that is enriched in OIS whereas it is not in RS in human cells (Kosar et al., 2011). Likewise, SASP varies according to the types of cells and stresses (Pérez-Mancera et al., 2014). Therefore, cellular senescence displays multiple heterogeneous characteristics depending on its context although it ultimately arrests cell cycle.

1.3.1: Replicative senescence

Historically, Leonard Hayflick and Paul Moorhead first discovered the restricted proliferative capacity in vitro by serial passaging in human fibroblasts, which was termed replicative senescence (RS) (Hayflick and Moorhead, 1961). Later, the cause of RS was found to be telomere

attrition (Harley et al., 1990). A telomere is a highly repetitive 5′-TTAGGG-3′ DNA sequence in vertebrates located at the tip of chromosomes, protecting chromosomes from chromosome loss, degradation, and end-to-end fusion (d'Adda di Fagagna, 2008). Despite its repeating identical DNA sequence, telomere remains stable and it does not trigger DDR in normal physiological condition. It is because telomere is shielded by proteins including telomeric repeat-binding factor 2 (TRF2) and protection of telomeres 1 (POT1), which together constitute the shelterin protein complex contributing to chromosome end protection (Denchi and de Lange, 2007; Karlseder et al., 2004). In human somatic cells, telomere length was reported to become progressively shorter, losing approximately 50-200 base pairs of telomeric DNA due to the lack of a template for DNA synthesis at the telomere when replicating nuclear DNA (d'Adda di Fagagna et al., 2003; Harley et al., 1990; Herbig et al., 2004). This end replication problem gives rise to telomere attrition, subsequently leading to the loss of interaction with the shelterin protein complex and enabling the access of DDR proteins, such as ataxia telangiectasia and Rad3-related (ATR) and ataxia-telangiectasia mutated (ATM) (d'Adda di Fagagna et al., 2003; Herbig et al., 2004). Consequently, critically shortened telomeres trigger DDR activation and the prolonged DDR signal confers permanent cell cycle arrest. Unlike the somatic cells, germline cells are eligible to replicate telomeres owing to telomerase. Telomerase is a ribonucleoprotein that contains catalytic protein, telomerase reverse transcriptase (TERT), which serves as a template for DNA synthesis at telomeres (Palm and de Lange, 2008). Therefore, telomerase expression allows germline cells to circumvent the telomere erosion. Supporting this finding, ectopic TERT expression rescued human somatic cells from telomere shortening and consequently replicative senescence, indicating that telomere attrition was an inducer of replicative senescence (Bodnar et al., 1998).

1.3.2. Oncogene-induced senescence

Not a long time from the discovery of RS, a novel mechanism of developing premature senescence was identified. In 1997, it was shown that human diploid fibroblasts and primary mouse embryo fibroblasts transduced with an oncogenic form of Ras allele (H-rasV12) underwent a permanent cell cycle arrest (Serrano et al., 1997). This research showed cells can prematurely promote the onset of senescence by tumorigenic gene expression. Moreover, further studies showed the activation of other Ras signalling pathways, such as BRAF, MEK, and Raf-1, resulted in premature senescence (Acosta et al., 2008; Lin et al., 1998; Zhu et al., 1998). This type of senescence is termed premature cellular senescence as it is independently established prior to the time point when RS is caused by telomere shortening (Campisi and d'Adda di Fagana, 2007). Oncogene-induced senescence (OIS) is one kind of premature cellular senescence induced by the activation of oncogenes or the inactivation of tumour suppressor genes. Hence, the development of OIS is distinct from replicative senescence, which was substantiated by the research that OIS was not rescued by the expression of telomerase (Jones et al., 2000). One of the functions of oncogenes is to encode proteins that stimulates cell growth. When they are upregulated in normal condition, it triggers DDR and subsequently cellular senescence in human cells (Bartkova et al., 2006; Di Micco et al., 2006). Conversely, the overexpression of oncogenes together with additional mutations of tumour suppressor or DDR genes can potentially transform cells from normal to malignant (Bartkova et al., 2006; Di Micco et al., 2006; Serrano et al., 1997). As a result, it enables cells to escape from cellular senescence, thereby becoming immortal and cancerous.

1.3.3. Secondary senescence

Secondary senescence refers to the type of senescence induced by interaction with neighbouring senescent cells. In contrast to replicative and oncogene-induced senescence which have primary insult, such as telomere attrition and active oncogene expression respectively, the

cause of secondary senescence is not well understood. Nevertheless, as of now, there are a number of studies that have determined secondary senescence is rather provoked from extant senescent cells via SASP or Notch signalling (Hoare et al., 2016; Parry et al., 2018; Teo et al., 2019). Hence, cell signalling is a key to facilitate secondary senescence. One study showed the development of secondary senescence by paracrine signalling using Transwell inserts that physically separated senescent cells from growing cells (Hoare et al., 2016). In addition, Hoare *et al*. revealed the transmission of senescence between adjacent cells was facilitated by Notch signalling, determining Notch signalling as an inducer of secondary senescence (Hoare et al., 2016). This type of senescence is also known as Notch-induced senescence (NIS) which is established in a juxtacrine manner (Hoare et al., 2016; Teo et al., 2019). NIS-induced cells are characterised by poor SAHF formation due to Notch signalling (Parry et al., 2018; Teo et al., 2019) and different gene expression profiles such as fibrillary collagen compared to OIS-induced cells (Teo et al., 2019), yet other features are largely undiscovered.

1.4. Nucleolus and ageing

As introduced in previous sections, senescence inducers such as abnormal oncogene expression and replicative stress can be sensed by nucleoli, resulting in nucleolar stress and subsequently cellular senescence. The oncogenic and replicative stress gives rise to morphological changes in nucleoli, which were determined through microscopic observation or immunofluorescence (Kuilman et al., 2010; Nishimura et al., 2015; Pinho et al., 2019; Serrano et al., 1997). Interestingly, nucleolar size has been associated with longevity across taxa. For example, mutations in slow growth suppressor 1 (SGS1; the gene encodes a RecQ helicase and homology to human WRN gene) in *Saccharomyces cerevisiae* gave rise to cells that were found to be prematurely aged and the old sgs1 cells represented nucleolar enlargement and fragmentation (Sinclair et al., 1997). Tiku *et al*. recently proposed that fibrillarin knockdown in *Caenorhabditis elegans*

led to smaller nucleoli and extended lifespan (Tiku et al., 2017). Moreover, they identified reduced nucleolar area in long-lived models of *Drosophila melanogaster*, mice in insulin signalling mutants with dietary restrictions, and humans who underwent dietary restriction and exercise (Tiku et al., 2017). In agreement with this discovery, primary fibroblasts derived from Hutchinson-Gilford progeria syndrome (HGPS) donors displayed enlarged nucleolar phenotype (Buchwalter and Hetzer, 2017). In addition, the enlarged nucleolar phenotype and escalated rRNA production were reported in line with normative ageing (Buchwalter and Hetzer, 2017). These findings support the idea that nucleolar size is conversely related to ageing.

Overall, a number of studies have proposed changes in nucleolar area or morphology along with signaling pathways in nucleolar stress and ageing. However, the alterations of nucleoli by different senescence inducers and associated genes are not well understood and substantiated. Therefore, in this research project, I ultimately aim to investigate the dynamic of the nucleolus in cellular senescence and identify differential gene expression linked with nucleolar dynamics.

Aims and Objectives:

The aims of this project is divided into three parts:

1) To investigate nucleolar dynamics in different types of senescence, namely, oncogene-induced, secondary, and replicative senescence.

2) To correlate intracellular changes inclduing nuclear size and SHAF formation with alterations in nucleoli in diverse types of senescence.

3) To examine the gene expression associated with enlarged nucleoli in oncogene-induced and replicative senescence

To achieve the aims above, the project is composed of three parts:

1) Nucleolar dynamics in oncogene-induced senescence

   The first section of this project involved the examination of nucleolar area in OIS. Furthermore, nuclear area was investigated and the link between nucleolar hypertrophy and SAHF formation was analysed. Finally, RNA-sequencing analysis was conducted to examine gene expression associated with nucleolar alterations in OIS.

2) Nucleolar dynamics in secondary senescence

   Nucleolar area was investigated in secondary senescence. Following that, an investigation of nuclear area was performed and the enrichment of SAHF formation was evaluated.

3) Nucleolar dynamics in replicative senescence

   Alterations in nucleolar area were analysed in RS. Subsequently, nuclear area was compared between young and old primary human cells and the association between nucleolar hypertrophy and SAHF formation was examined. Lastly, RNA-seq data was analysed to examine gene expression linked with nucleolar enlargement in RS.

Chapter II

Materials and Methods

2.1: Cell culture:

2.1.1: Co-culture system for the induction of oncogene-induced senescence and secondary senescence:

Co-culture system refers to the cell culture of two or more different types of cells in one dish, allowing for sharing of the media as well as growth factors. To comply with the purpose of the project, IMR90 human fibroblasts transduced with the human H-RasV12 oncogene (ER:Ras IMR90) were co-cultured with IMR90:YFP empty vector fused to Venus protein (mVenus:EV), thereby expressing yellow fluorescent protein (YFP). Here, ER:Ras IMR90 cells were used for identifying nucleolar dynamics in OIS while mVenus:EV cells were used to determine nucleolar dynamics in secondary senescence. Prior to co-culture, ER:Ras IMR90 and mVenus:EV were separately cultured in 10cm Corning cell culture dishes in Dulbecco's Modified Eagle's medium (DMEM, Gibco) supplemented with 100mM sodium pyruvate (Gibco), 1% Minimum Essential Medium Non-Essential Amino Acid (MEM NEAA) solution (Gibco), 1% Penicillin Streptomycin 10,000U/ml (Gibco), 1% antibiotic-antimycotic 100X solution (Gibco), 2-mercaptoethanol 50mM (Gibco), and 10% foetal calf serum (FCS) at 37℃ with 5% CO_2. They were separately passaged twice before starting co-culture. When cells achieved 80% or above confluency, the number of cells were examined in both ER:Ras IMR90 and mVenus:EV to culture the cells together with the ratio of 5:1 (Figure 4). To stimulate OIS, 100nM of 4-hydroxytamoxifen (4-OHT) was added, which caused the activation of the Ras oncogene in ER:Ras IMR90. The potential development of secondary senescence in mVenus:EV was induced by interaction with ER:Ras IMR90 cells whose Ras oncogene was activated. The co-culture system allowed for cell-cell communication to establish secondary senescence. Co-cultured cells were incubated with 4-OHT for varying periods of time: two, four, or seven days

(referred to as day 2, day 4, and day 7 cells respectively according to 4-OHT incubation time) (Figure 4). This time-course experiment allowed the determination of nucleolar dynamics in the course of OIS and secondary senescence. Co-culture dishes without the supplement of 4-OHT were used as control.

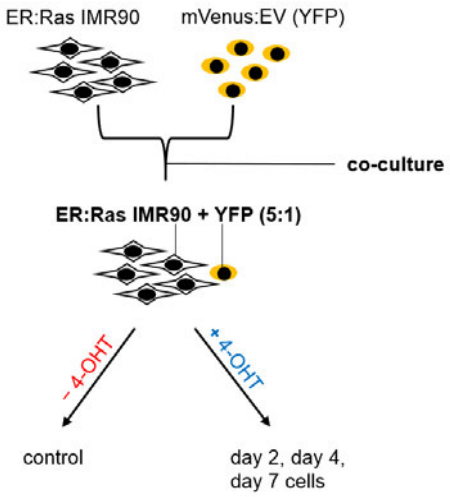

Figure 4: Co-culture system used for the induction of oncogene-induced and secondary senescence: ER:Ras IMR90 cells were co-cultured with mVenus:EV with a ratio of 5:1. The co-culture system allowed for simultaneous OIS and secondary senescence upon the treatment of 4-OHT. Different time periods of 4-OHT incubation were used, from two, four, or seven days, to conduct time-course experiment. Co-cultured cells without 4-OHT treatment were used as control.

2.1.2: Cell culture for the induction of replicative senescence:

IMR90 human fibroblasts were cultured in 10cm Corning cell culture dishes in DMEM (Gibco) supplemented with 100mM sodium pyruvate (Gibco), 1% MEM NEAA solution (Gibco), 1% Penicillin Streptomycin 10,000U/ml (Gibco), 1% antibiotic-antimycotic 100X solution (Gibco), 2-mercaptoethanol 50mM (Gibco), and 10% FCS at 37℃ with 5% CO_2. To establish replicative senescence (RS), long-term serial cell passaging was performed. Initially, IMR90 human fibroblasts (passage number = 15; P15) were cultured until achieving 80% or above confluency. Once confluent, the number of cells from one dish were investigated and the cells were subsequently transferred into three new

dishes and cultured. This was repeated when 80% or more confluency was achieved and the cultures split to a 1:3 ratio until the time that IMR90 human fibroblasts developed RS (passage number = 24; P24). The remaining cells from cell culture were frozen and stored for further experiments.

2.2: Cell proliferation assay

2.2.1: EdU incorporation assay:

An EdU incorporation assay was performed to determine the proportion of proliferative cells. IMR90 human fibroblasts or the co-culture of ER:Ras IMR90 and mVenus:EV cells from 10cm Corning cell culture dishes were transferred onto 22mm x 22mm coverslip in 6-well plates and left to incubate for overnight at 37℃ and 5% CO_2. Cells were then incubated with 10μM of EdU solution for 12 hours to enhance the identification of senescent cells from the cell population. Cells were then fixed with 4% paraformaldehyde (PFA) for 15 minutes and subsequently washed twice in 3% of bovine serum albumin (BSA) in PBS. The permeabilisation of the cell membrane was achieved by incubating with 0.2% Triton X-100/PBS for 20 minutes at room temperature. The permeabilisation buffer was aspirated and cells were washed twice with 3% BSA in PBS. The reaction cocktail of Click-iT™ EdU was prepared as described in the protocol (ThermoScientific). Cells were incubated with 0.5ml of Click-iT™ reaction cocktail for 30 minutes and the 6-well plates were wrapped with foil to avoid light. Cells were then washed with 3% BSA in PBS to eliminate any trace of Click-iT™ reaction cocktail. Coverslips were then mounted onto slides with a drop of VECTASHIELD® (Vector Laboratories) mounting medium supplemented with 1mg/ml 4',6-diamidino-2-phenylindole dihydrochloride (DAPI). The four edges of glass coverslips were sealed with nail polish before image acquisition.

Because of insufficient reaction components from Click-iT™, I also used alternative methods and materials to prepare for Click reaction mix (Table 1). This alternative reaction mix only substituted the reaction

cocktail of Click-iT™ EdU and the rest of EdU assay protocol was identically followed as described above.

Reaction components	Volume (µl)
Dulbecco's Phosphate-Buffered Saline (DPBS)	2220
200µM $CuSO_4$	25
Alexa Flour® 555	5
200mg/ml L-asconbade acid	250

Table 1: An alternative reaction mix prepared for EdU incorporation assay: The volume used in this table was a reaction mix for incubating five coverslips. Note that 200mg/ml L-asconbade acid was freshly prepared and it was added into the reaction mix just prior to incubation with cells.

2.2.2: Cell count:

IMR90 human fibroblasts were washed twice with Dulbecco's Phosphate-Buffered Saline (DPBS) (Gibco) and they were subsequently trypsinised with 0.25% Trypsin-EDTA 1X solution (Gibco). Following trypsinisation, cells were collected into 15ml conical tube and centrifuged for 4 minutes at 1300 revolutions per minute (rpm). Supernatant was aspirated and the pellet then mixed with 1ml of cell-culture medium to make a cell suspension. 10µl of cell suspension and 10µl of trypan blue were blended in Eppendorf tube and 10µl of mixture was pipetted into a Countess chamber slide and inserted in a Countess II automated cell counter. A total cell count and culture period was measured for every passage to examine the exhibition of RS (Table 2).

Passage number	Total cell count (cells/ml)	Culture period (days)
15	$1.61*10^6$	0
16	$2.48*10^6$	7
17	$3.17*10^6$	6
18	$3.18*10^6$	6
19	$3.66*10^6$	6

20	$2.53*10^6$	10
21	$1.17*10^6$	7

Table 2: The total number of cells and culture period recorded during long term serial passage of IMR90 cells: In the middle of the project, cells were inevitably frozen at passage number 21 before they achieved 80% confluency and were then thawed to continue the experiment which led to disrupted cellular stability. As a consequence, the data from passage 22 to 24 were excluded from cell count analysis.

Due to replicative exhaustion, cells with old passage numbers are inclined to lose replicative capability, thereby identifying as a growth plateau in accumulated cell count over total culture period. To measure the accumulated cell count, the number of cells seeded in one cell culture dish was firstly calculated through dividing the total number of cells by three because IMR90 human fibroblasts were split in the ratio of 1:3 for every passage (Table 3). The number of cells seeded in one dish were then subtracted from the total number of cells from following passage to acquire the number of proliferated cells before passaging (Table 3). Finally, the accumulated cell counts were obtained by adding up the number of progeny cells from each passage (Table 4). Similarly, the total culture period was calculated by adding up the culture period between passages (Table 4).

Passage number	**The number of cells seeded in one dish (cells)**	**The number of progeny cells (cells)**
16	$0.53*10^6$	$1.95*10^6$
17	$0.83*10^6$	$2.34*10^6$
18	$1.06*10^6$	$2.12*10^6$
19	$1.06*10^6$	$2.60*10^6$
20	$1.22*10^6$	$1.31*10^6$
21	$0.84*10^6$	$0.33*10^6$

Table 3: The number of cells seeded in one cell culture dish and the number of proliferated cells identified prior to passaging

Passage number	Accumulated cell counts (cells)	Total culture period (days)
15	0	0
16	$1.95*10^6$	7
17	$4.29*10^6$	13
18	$6.41*10^6$	19
19	$9.01*10^6$	25
20	$10.32*10^6$	35
21	$10.65*10^6$	42

Table 4: The accumulated cell counts and total culture period during IMR90 serial passaging: The total number of cells at the first passage was defined as 0 because it was the start point of serial passaging.

2.3: Nucleoli staining:

2.3.1: Antibody concentration optimisation:

Prior to immunofluorescence, antibody concentration was optimised to enhance the quality of nucleolar staining and to decrease the non-specific staining of background. IMR90 human fibroblasts were seeded onto 22mm x 22mm coverslip in 6-well plates and incubated overnight at 37℃ and 5% CO_2. Cells were fixed with 80% methanol for 5 minutes and washed with Phosphate Buffered Saline with Tween 20 (PBST). The coverslips were then incubated with 0.1% PBST for 20 minutes at room temperature to permeabilise the cell membrane and subsequently washed by PBST. Cells were treated with 1% BSA-PBST/10% normal goat serum for one hour to block non-specific molecular binding such as protein-protein interaction. The blocking solution was aspirated and cells were washed with PBST. Different dilution factors were used to prepare different concentration of anti-fibrillarin antibody (ab184817, Abcam) (Table 5). 100µl of antibody was added to cells that were incubated for 30 minutes covered with aluminium foil to generate a light-protective environment. Cells were

washed with PBST and coverslips were mounted on glass slides onto VECTASHIELD® (Vector Laboratories) drop containing 1mg/ml DAPI.

For anti-fibrillarin antibody (ab4566, Abcam) and goat anti-mouse IgG 555-conjugated (AnaSpec) were previously optimised from Tamir Chandra's research group and therefore I followed the dilution factor of 1 in 200.

Dilution factor	Antibody preparation
1 in 50	4.2µl of antibody + 205.8µl of PBST
1 in 100	100µl of diluted antibody (1 in 50) + 100µl of PBST
1 in 200	100µl of diluted antibody (1 in 100) + 100µl of PBST
1 in 400	100µl of diluted antibody (1 in 200) + 100µl of PBST

Table 5: Dilution factor used for preparing antibody with different concentration: Antibody was diluted with PBS according to dilution factor.

2.3.2: Immunofluorescence:

IMR90 human fibroblasts or the co-culture of ER:Ras IMR90 and mVenus:EV cells were seeded onto 22mm x 22mm coverslips in 6 well plates and left to incubate overnight at 37℃ with 5% CO_2. Cells were fixed with 4% PFA for 15 minutes and washed twice with PBS, then incubated in 0.2% Triton-X in PBS for 5 minutes at room temperature to permeabilise the cell membrane. Cells were washed twice with PBS and 100µl of anti-fibrillarin antibody (ab4566, Abcam), diluted 1:200 in PBST, was added for incubation for 45 minutes at room temperature (Table 6). After incubating with the fibrillarin antibody, cells were washed twice with PBST and incubated with 600µl of goat anti-mouse IgG 555-conjugated (AnaSpec) secondary antibody, diluted 1:200 in PBST, for 45 minutes at room temperature. These were kept in the dark to avoid light exposure and bleaching of staining (Table 6). The secondary antibody was discarded and cells were washed with PBST for 10 minutes and repeated three times. The coverslips were mounted on a glass slide with a drop of VECTASHIELD® (Vector Laboratories)

containing with 1mg/ml DAPI. Subsequently, coverslips were sealed by nail polish for imaging acquisition.

For immunofluorescence with anti-fibrillarin antibody (ab184817, Abcam), IMR90 human fibroblast cells were fixed with 80% methanol. Fixative solution was removed and cells were washed with PBST. Following the aspiration of PBST, 0.1% PBST was added and incubated for 20 minutes for permeabilisation. The permeabilisation buffer was discarded and cells were washed with PBST and subsequently treated with 1% BSA-PBST/10% normal goat serum for one hour. Afterwards cells were washed with PBST, they were then incubated with 100µl of antibody, diluted 1:50 in PBST, for 30 minutes at room temperature and placed in a foil sealed container to inhibit photo-bleaching (Table 6). The antibody was conjugated with fluorescence protein and therefore it did not require secondary antibody. Cells were washed with PBST and the coverslips were mounted on glass slides with the drop of VECTASHIELD® (Vector Laboratories) containing 1mg/ml DAPI. Prior to image acquisition, the coverslips were sealed with nail polish.

Antibody type	Antibody name	Company	Species
Primary antibody	Anti-fibrillarin antibody (ab184817)	Abcam	Rabbit
	Anti-fibrillarin antibody (ab4566)	Abcam	Mouse
Secondary antibody	Goat anti mouse (Alexa Flour® 555)	AnaSpec	Goat

Table 6: Antibodies used for immunofluorescence

2.4: Image acquisition:

Following EdU incorporation assay, antibody optimisation, and immunofluorescence, cells were visualised by epifluorescent microscope using 40x magnification and multidimensional acquisition via Micro-Manager software (v 1.14). To scan multiple fluorescence

channels such as DAPI, YFP-mVenus, and EdU Alexa Flour® 555, the triple channel of DAPI, FITC, and Texas Red were used. In addition, antibodies used in immunofluorescence were identified according to fluorescent signals employed in cells and different exposure values were set (Table 7).

Channel	Anti-fibrillarin antibody (ab184817)	Anti-fibrillarin antibody (ab4566) with goat anti mouse (Alexa Flour® 555)
DAPI	100	150
FITC	100	200
TxRd	N.A.	100

Table 7: Exposure values to acquire immunofluorescence images: Multiple channels were used to detect different fluorescent signals. Specific emission and excitation filters were selected for each fluorochrome. N.A. refers to not applicable.

2.5: Image sorting and quantification

2.5.1: Image sorting

Prior to quantification, immunofluorescence images of co-cultured cells were grouped according to 4-OHT incubation days (i.e. control, day 2, day 4, and day 7). To isolate individual cell images from co-cultured cell population images, the individual cell image was selected, cropped, and duplicated via ImageJ tools and separately saved in Tiff format. Subsequently, the individual cell images were sub-grouped by cell types, ER:Ras IMR90 and mVenus:EV, which were used for analysing nucleolar and nuclear size at different time points of OIS or secondary senescence. To assess the association between nucleolar hypertrophy and senescence-associated heterochromatin foci (SAHF) formation, the sub-grouped images of cells were separated based on SAHF formation. EdU assay images were initially grouped between control and day 7 co-cultured cells. The individual cell images of EdU assay

were produced using ImageJ tools and they were divided based on EdU incorporation, which were further sub-grouped by SAHF formation.

The immunofluorescence images of IMR90 human fibroblasts were separated between early and late passage (i.e. P17 and P24). Likewise, the EdU assay images of IMR90 fibroblasts were grouped by passage number and sub-grouped by the status of EdU staining.

2.5.2: Quantification by CellProfiler:

DAPI, FITC, and Texas Red channels were processed by CellProfiler (Broad Institute, v 4.0.3), giving the ability to quantify the size of nucleoli and nuclei. However, the resultant AreaShape by CellProfiler quantification has the unit of pixels, instead of μm^2. To convert the unit to μm^2, 1 pixel value needs to be calculated. Firstly, the number of pixels per micron detected in images was determined by checking the information from Scale under Analyse tab in ImageJ. As a consequence of identification, 1 micron was 6.2499 pixels in author's imaging acquisition setting. To obtain the value of $1\mu m^2$, 6.2499 was squared, resulting in 39.06125. Finally, the AreaShape was divided by 39.06125 and that led to nucleoli or nuclei size with the unit of μm^2.

2.5.3: Quantification by ImageJ:

ImageJ was used as a complementary method to measure and quantitate the nucleoli and nuclei of cells. The boundary of DAPI-negative regions were marked and measured for nucleolar size whereas DAPI-staining regions were quantified for nuclear area. To enhance the marking accuracy, images were magnified by between 150 and 300 percent. Polygon selection from ImageJ was used to manually mark the nucleoli and nuclei and their size was quantified by ImageJ. All measured values by ImageJ were in μm^2.

2.5.4: Quantitatation of images from external sources

Images of co-cultured cells, ER:Ras IMR90 and mVenus:EV, were adopted from external sources (more specifically, they originated from my bachelor's project experiments) and they were used for quantifying nucleolar and nuclear size and investigating the link between nucleolar expansion and SAHF in OIS. The co-cultured cells were stained with COL1A2 or Jagged1 antibody respectively (the images of cells are referred to as Col and Jag image respectively, according to antibody stain for cells) instead of fibrillarin, which were not nucleolar markers. Therefore, the Col and Jag images were analysed by ImageJ alone due to lack of nucleolar staining that is required for quantification by CellProfiler. Consistent with the condition used for project experiment, the co-cultured cells were incubated with 100nM of 4-OHT to cause OIS and secondary senescence and different 4-OHT incubation times were applied to, for example, two, four, or seven days. Identical procedures were taken to harvest quantitative nucleolar area as described in section 2.5.3.

2.6: RNA sequencing and RNA sequencing analysis:

The data of RNA sequencing (RNA-seq) was generated by the research group of Dr. Peter D. Adams (Rai et al., 2014). Subsequently, quality control, trimming, and read alignment was performed by Neil Robertson from Dr. Tamir Chandra's research group. SeqMonk software (http://www.bioinformatics.babraham.ac.uk/projects/seqmonk) was used for importing quality-controlled and aligned read (bam) files. The data was initially quantified at the mRNA level using RNA-seq quantitation pipeline and then match distribution quantitation was further used. Protein coding mRNA was searched via the find feature in SeqMonk and the resultant data was saved as annotation track. Filtering tool (filtering on values) was used to generate probe lists from protein coding mRNA. Following filtering, the protein coding mRNA was quantified by RNA-seq quantitation pipeline to generate raw counts. DESeq2 statistical test was performed (p=0.05 with multiple testing correction) to identify differential gene expression and

subsequently the data was transformed in log scale. Lastly, genes of interest (table 9) were examined via the find feature in SeqMonk and the data was visualised by R (v 4.0.3).

2.7: Statistical analysis:

Student's t-test and one way ANOVA followed by Tukey's HSD test were performed by R (v 4.0.3) where appropriate. P-values lower than 0.05 were considered as statistically significant and they were symbolised with either ns or an asterisk according to the degree of significance (Table 8). Pearson correlation test was used to investigate the correlation coefficient between the measurement of nucleolar area by CellProfiler and ImageJ to confirm ImageJ as a complementary method for quantitating nucleolar size.

Symbol	P-value
ns	p>0.05
*	p≤0.05
**	p≤0.01
***	p≤0.001

Table 8: P-values in line with symbols used to determine statistical significance

Chapter III

Results

Nucleolar Dynamics in Oncogene-Induced Senescence

3.1: Oncogene-induced senescence was caused by 4-OHT

To examine nucleolar dynamics in oncogene-induced senescence (OIS) and secondary senescence, a co-culture system was employed as described in Materials and Methods using ER:Ras IMR90 and mVenus:EV (Figure 4). Following co-culture, co-cultured cells were treated with 4-hydroxytamoxifen (4-OHT) to induce OIS. 4-OHT incubation leads to Ras activation in ER:Ras IMR90 cells because of the inducible ER:Ras construct transduced in IMR90 fibroblasts; the overexpression of Ras eventually triggers OIS. Co-cultured cells were incubated with 4-OHT for different periods, such as two, four, or seven days (the co-cultured cells were referred to as day 2, 4, or 7 cells according to the time period of 4-OHT treatment), in order to observe nucleolar dynamics within different time frames in OIS and secondary senescence respectively. Co-cultured cells without 4-OHT treatment were used as control.

Firstly, proliferative capacity was investigated by 5-ethynyl-2′-deoxyuridine (EdU) assay. EdU is a thymidine analogue that incorporates into DNA once DNA is replicated, thereby enabling the author to distinguish proliferative cells from the cell population. To enhance the identification of senescent cells, 12 hours of EdU incubation was employed and EdU incorporation rate was compared between the control and day 7 ER:Ras IMR90. Only 5% of day 7 ER:Ras IMR90 cells were EdU-incorporated, which was significantly lower ($p<0.001$), compared to the control that had about one third EdU-positive cells (Figure 5A and B). This indicates a significant decrease in proliferating cells and therefore that OIS was established by 4-OHT treatment.

(A)

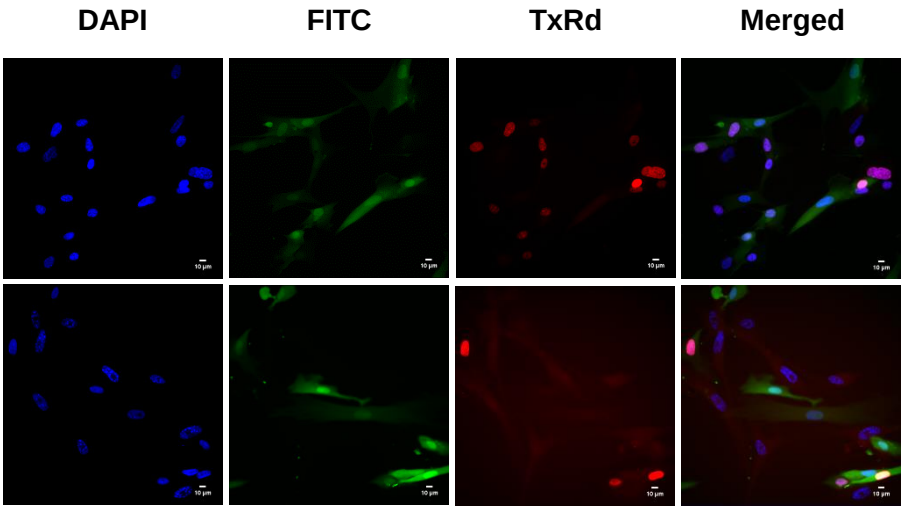

(B)

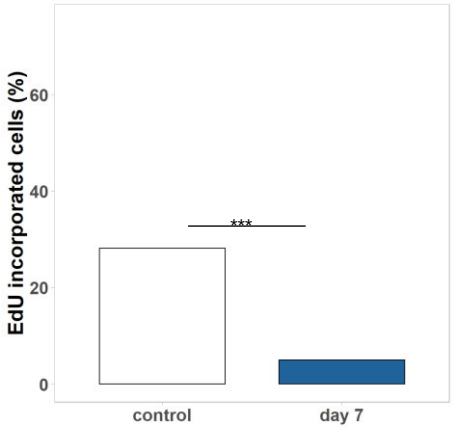

Figure 5: EdU incorporation assay of ER:Ras IMR90. (A) The control (images from the first row) and day 7 co-cultured cells (images from the last row) were subjected to EdU incorporation for 12 hours. The images were visualised by epifluorescent microscope with x40 magnification. The scale bar is 10 µm. (B) After 4-OHT treatment for 7 days, EdU-positive ER:Ras IMR90 cells were significantly reduced ($p<0.001$). Data was analysed by student's t-test. n=137 for EdU-incorporated cells in control (total number of cells = 487 cells) and n=25 for EdU-positive cells in day 7 (total number of cells = 497 cells).

3.2: Examination of nucleolar area in oncogene-induced senescence

3.2.1: Nucleolar area quantitated by CellProfiler

Following the identification of OIS in ER:Ras IMR90, changes in nucleolar area in response to oncogene activation were examined. Immunofluorescence by anti-fibrillarin antibody (ab4566, Abcam) with goat anti mouse (Alexa Flour® 555) secondary antibody was performed as described in Methods and Materials to stain nucleoli. Several markers are well known to define nucleoli including fibrillarin, upstream binding factor (UBF), nucleolin, nucleophosmin, and MYBBP1A. Fibrillarin is a nucleolar protein enriched in DFC and engaged in rRNA maturation and ribosome biogenesis and thus it was considered as a good nucleolar marker (Hayashi et al., 2018; Tiku et al., 2017; Yang et al., 2018). After image acquisition, CellProfiler was employed and images were subsequently processed to measure nucleolar and nuclear area respectively (Figure 6). The quantified nucleolar area by CellProfiler was in the units of pixels and therefore it was converted to μm^2 as described in Methods and Materials.

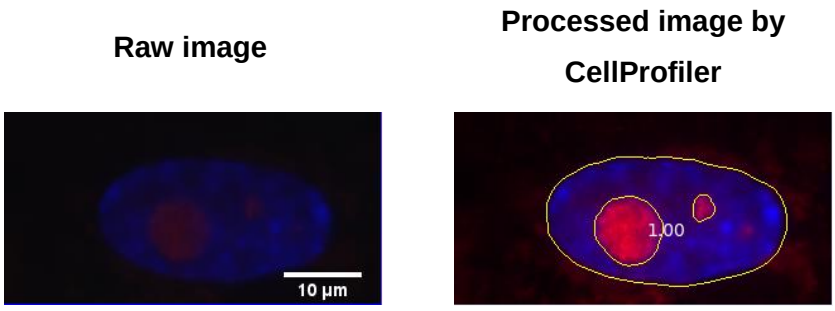

Figure 6: Nucleolar and nuclear area measured by CellProfiler. ER:Ras IMR90 cells were subjected to immunofluorescence and the nucleus was defined by DAPI staining. Cell images were captured by epifluorescent microscope with x40 magnification. Subsequent to image acquisition, images were processed by CellProfiler that marked and quantified the regions of nucleoli and nuclei respectively. A number (shown as 1.00) was conferred to each nucleus after the cell image was processed by Cellprofiler to track the origin of nucleoli from different nuclei.

3.2.2: Nucleolar area quantitated by ImageJ

While acquiring EdU-incorporated cell images by microscopy, I noticed the nucleoli were contrasted with the DAPI-stained nucleus. Therefore, they seemed to be reflected as DAPI-negative regions (Figure 7A). Likewise, the observation of images from external sources (Col and Jag image as described in section 2.5.4 in Methods and Materials) led to the identification of the nucleolar area as a DAPI-negative region (Figure 7A). Subsequent to the observation of different sets of images, I wondered if the measurement of DAPI-negative regions by ImageJ could be used as a complementary method to CellProfiler to quantify nucleolar area. To verify the hypothesis, the correlation coefficient between CellProfiler and ImageJ was examined by Pearson correlation test. In essence, the equivalent nucleolar area measured by two different methods were compared. If there is a high correlation coefficient, it likely suggests the measurement of DAPI-negative area by ImageJ closely matches with nucleolar area quantitated by CellProfiler.

Firstly, the fluorescent channels of fibrillarin-stained cell images were split to obtain the images of DAPI channel alone (Figure 7B). All images from the time-course experiment, such as control, day 2, 4, and 7 were used for the Pearson correlation test in order to evaluate the consistency and accuracy of DAPI-negative area quantitation by ImageJ. Following the acquisition of images with DAPI channel alone, DAPI-negative regions in nuclei were measured by ImageJ as described in Methods and Materials (Figure 7B). The individual resultant nucleolar area was compared with the corresponding nucleolar area quantified by CellProfiler (Figure 7B). Surprisingly, a strong positive linear relationship was identified across all time-course data (correlation coefficient>0.7 and $p<0.05$), indicating the measurement of DAPI-negative area by ImageJ was sufficient to alternatively quantify nucleolar area (Figure 8). More importantly, it permitted author to quantitate nucleolar area without using nucleolar markers. In other words, images from the EdU assay and external sources (i.e. Col, and Jag images) were also able to be used for

analysing nucleolar area via ImageJ. In conclusion, CellProfiler together with ImageJ were used to quantify nucleolar area to examine the dynamics of the nucleolus in different types of senescence.

(A)

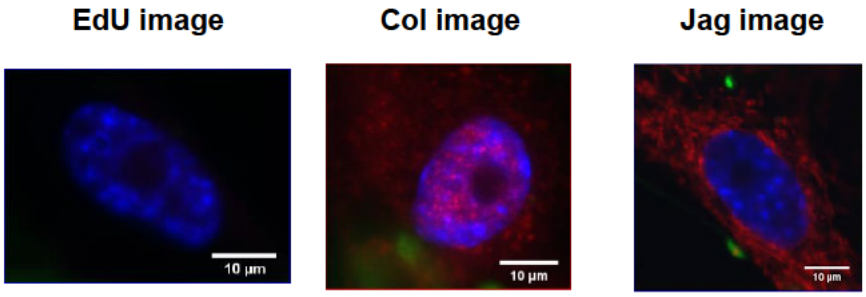

(B)

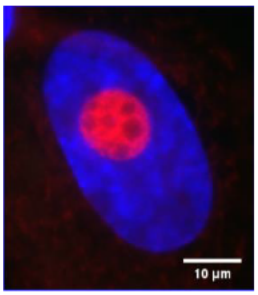

The image of ER:Ras IMR90 stained with anti-fibrillarin antibody and secondary antibody (Alexa Flour® 555). The nucleus was stained with DAPI.

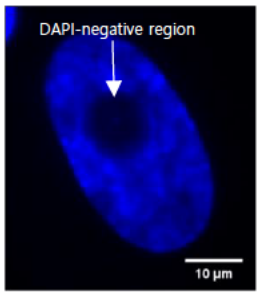

The fluorescent channels were split, resulting in the image with DAPI channel alone. The nucleolar area was reflected as a DAPI-negative region.

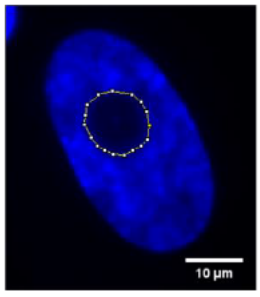

The nucleolus was marked by ImageJ and the area was subsequently quantified.

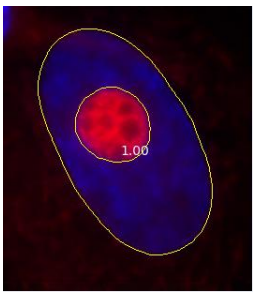

The equivalent cell image processed by CellProfiler was used for the Pearson correlation test.

Figure 7: Nucleolar area measurement by ImageJ. (A) An observation from different sets of images identified that nucleoli were shown as DAPI-negative areas in DAPI-stained nucleus. (B) ImageJ was initially used to acquire an image with DAPI channel alone. The image was subsequently used for marking and quantifying the area of nucleolus and the nucleolar area was compared with the corresponding nucleolus quantitated by CellProfiler.

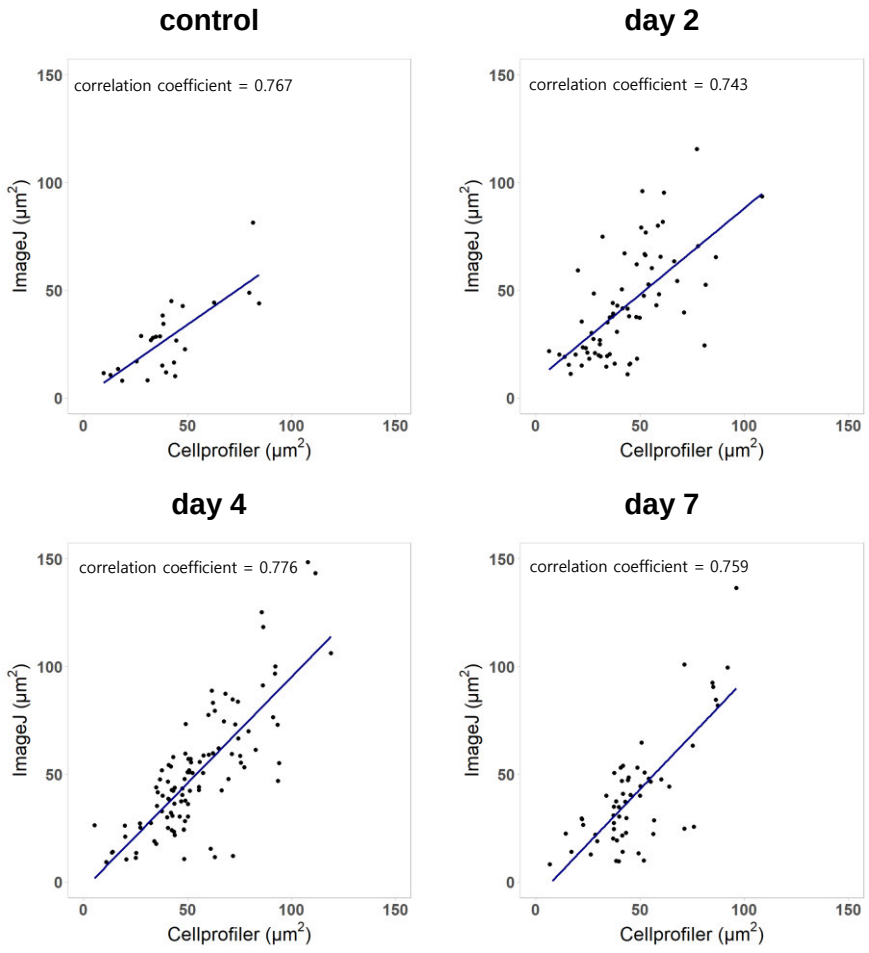

Figure 8: Correlation coefficient between CellProfiler and ImageJ. The Pearson correlation test was performed to examine the correlation coefficient between CellProfiler and ImageJ. Nucleolar area quantified by CellProfiler and ImageJ was found to be significantly correlated (correlation coefficient>0.7, p<0.05). A strong linear relationship suggests the quantitation of DAPI-negative region by ImageJ was a decent method to alternatively measure nucleolar area. Student's t-test was used to analyse the data. n=25, 70, 101, and 57 for control, day 2, 4, and 7 respectively.

3.2.3: Nucleolar area was significantly increased by oncogene-induced senescence

To begin with, nucleolar area in control and day 7 ER:Ras IMR90 cells was examined by immunofluorescence with a fibrillarin antibody (ab4566, Abcam) with a goat anti mouse (Alexa Flour® 555) secondary antibody and subsequent analysis was conducted using CellProfiler. Significantly increased nucleolar area was identified in day 7 cells ($p<0.001$), which was enlarged by 53.84μm^2 on average. However, cells without 4-OHT treatment had a mean nucleolar size of 32.94μm^2, suggesting nucleolar enlargement was caused by OIS (Figure 9A). Likewise, the quantitation of nucleoli by ImageJ revealed a corresponding result, a significant increase in the mean of nucleolar size from 19.66μm^2 to 41.33μm^2 upon OIS establishment in day 7 ER:Ras IMR90 cells ($p<0.001$) (Figure 9B). Together, these results indicate nucleolar hypertrophy was triggered by OIS.

(A) (B)

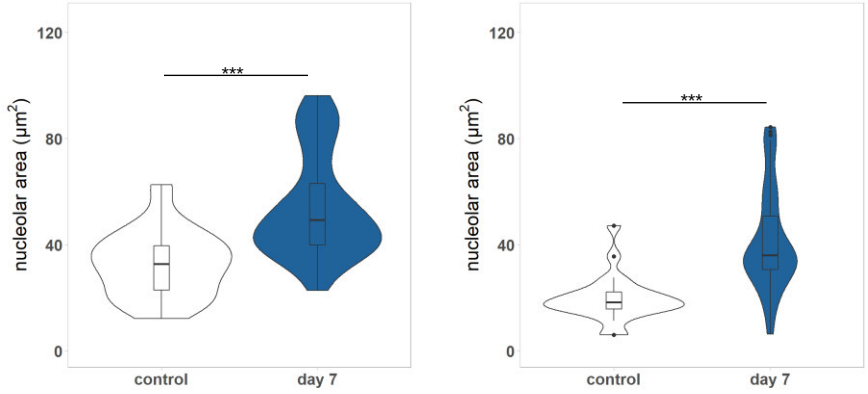

Figure 9: Nucleolar area was significantly enlarged in day 7 ER:Ras IMR90. (A and B) Nucleolar size was examined by CellProfiler and ImageJ respectively. Nucleolar area in day 7 ER:Ras IMR90 was significantly enlarged ($p<0.001$), suggesting OIS caused nucleolar hypertrophy. Student's t-test was performed to analyse the data. (A) n=34 and 50 for control and day 7. (B) n=24 and 52 for control and day 7.

The confirmation of nucleolar enlargement in day 7 ER:Ras IMR90 by oncogenic stimuli led to a question: when could changes in nucleolar area be observed in the process of OIS. To answer the question, a time-course experiment was conducted by treating the cells with 4-OHT for different numbers of days, such as two, four, or seven days (referred to as day 2, 4, or 7 cells according to the period of 4-OHT incubation). The time-course experiment was expected to confer an idea of the dynamics of changes in nucleolar area during OIS. Immunofluorescence by anti-fibrillarin and secondary antibody was performed (Figure 10) and nucleolar area was quantitated by CellProfiler. Interestingly, nucleolar size became significantly greater from day 2 ($p<0.001$) (Figure 11A). Similarly, nucleolar area measured by ImageJ identified a significant increase in nucleolar size from day 2 onwards ($p<0.05$) (Figure 11B). This likely suggests changes in nucleolar area were induced at an earlier timepoint in response to oncogene activation. Notably, heterogeneous nucleolar area was observed within day 2, 4, and 7 cell populations, generally in the range of $10\mu m^2$ to $100\mu m^2$ (Figure 11A and B). Such a wide variety of nucleolar area may indicate nucleoli respond distinctively to oncogenic stress and genes associated with nucleolar integrity are possibly expressed differently to some extent among cells.

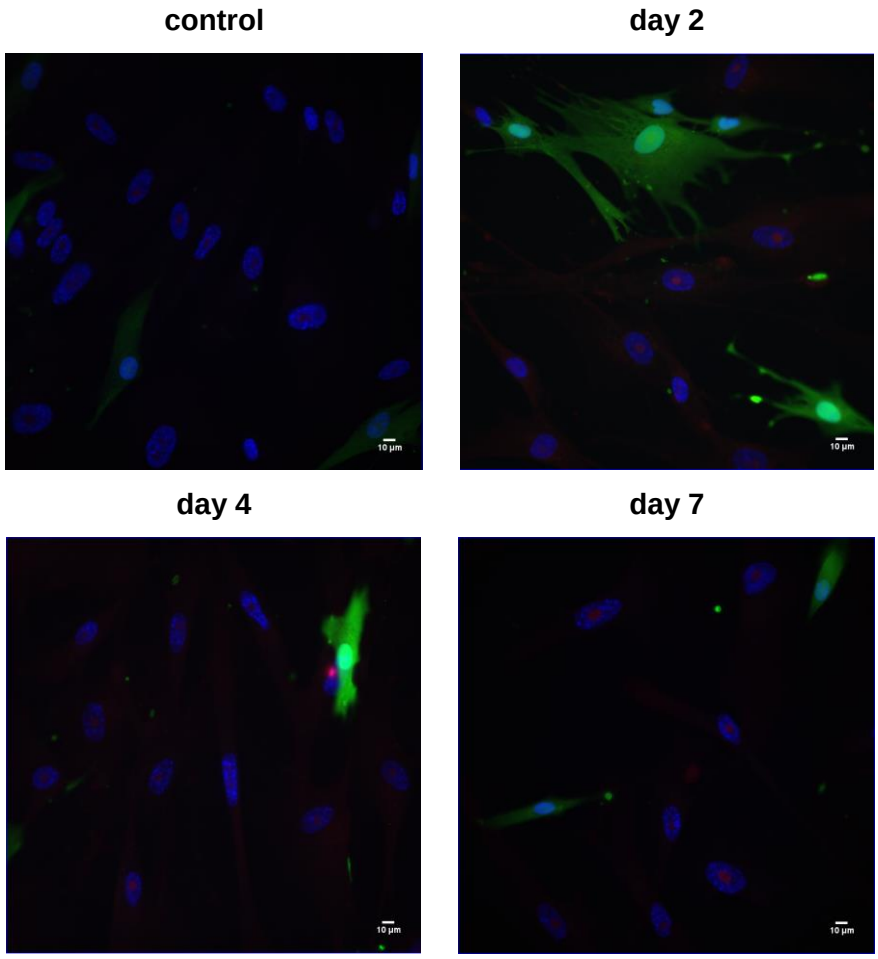

Figure 10: Immunofluorescence images of co-cultured ER:Ras IMR90 and mVenus:EV. Immunofluorescence was conducted using fibrillarin antibody (ab4566, Abcam) and secondary antibody (Alexa Flour® 555). Images were visualised by epifluorescent microscope with x40 magnification. The scale bar represents 10µm.

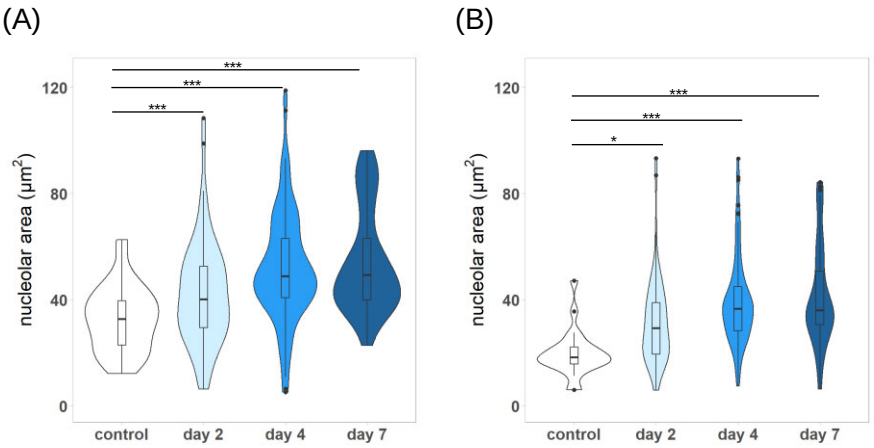

Figure 11: Investigation of nucleolar area at different time point during OIS. (A and B) Time-course experiment allowed for the examination of nucleolar area in the course of OIS. Nucleolar area was found to be significantly altered from day 2 onwards ($p<0.05$). The data was analysed by one-way Anova followed by a post-hoc Tukey's HSD correction. (A) n=34, 64, 86, and 50 for control, day 2, 4, and 7 respectively. (B) n=24, 31, 82, and 52 for control, day 2, 4, and 7 respectively.

To further confirm the alterations in nucleolar area in the time course of OIS, images from external sources (described in section 2.5.4 in Methods and Materials) were analysed by ImageJ. As previously described, DAPI-negative regions were quantitated. In agreement with the previous results, nucleolar size was significantly augmented in day 7 cells ($p<0.001$), indicating OIS caused alterations in nucleolar area. Moreover, oncogenic stress induced a significant nucleolar expansion from day 4 onwards ($p<0.001$) (Figure 12A and B). This suggests nucleolar expansion was caused at early timepoint of OIS between day 2 and 4. A great variation in nucleolar size was also determined across all groups of data.

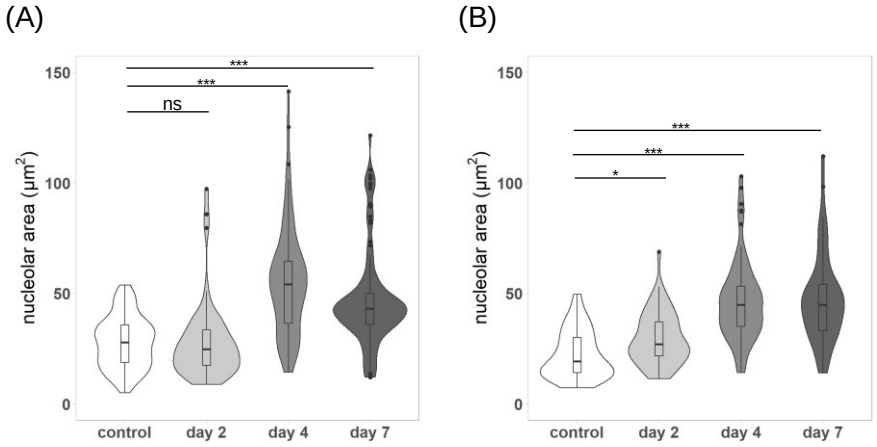

Figure 12: Nucleolar area examination in the time course of OIS. (A and B) Nucleolar area was examined at different timepoints of OIS. Nucleolar area was significantly enlarged from day 4 ($p<0.001$), but before this might be too early to examine alterations in nucleolar area. One-way Anova followed by a

post-hoc Tukey's HSD correction was applied for data analysis. (A) n=76, 52, 79, and 116 for control, day 2, 4, and 7 respectively. (B) n=83, 53, 79, and 51 for control, day 2, 4, and 7 respectively.

Lastly, ER:Ras IMR90 images from the EdU assay were analysed by ImageJ to validate an increase in nucleolar area by OIS. DAPI-negative area was measured and quantified by ImageJ. One of the advantages to analysing cell images produced by EdU assay is that it is feasible to distinguish proliferative cells from cell population owing to EdU incorporation. Unlike with EdU images, examining immunofluorescence images did not make it possible to clearly distinguish proliferative or senescent cells from the cell population. Therefore, using EdU images will likely enhance the possibility of investigating nucleolar size in two discrete cell populations, proliferative versus senescent cell populations. Firstly, difference in nucleolar area between control and day 7 ER:Ras IMR90 was inspected. Consistent with the earlier results, nucleolar area was significantly enlarged from 13.16μm^2 to 33.07μm^2 on average ($p<0.001$) (Figure 13A), which confirmed nucleolar enlargement was caused by oncogenic stress. Then, nucleolar area was compared between day 7 EdU-positive and day 7 EdU-negative ER:Ras IMR90. In other words, nucleolar area was compared between proliferative and senescent cells within the day 7 cell population. A significant increase in nucleolar area was determined in EdU-negative cells ($p<0.001$) (Figure 13B), likely implying nucleolar hypertrophy was induced upon developing OIS. It is important to note that there was a low number of day 7 EdU-positive cells (n=18) due to the long period of 4-OHT incubation, which restricted the generation of numerous proliferative cells. Taken together, these results show that OIS triggered nucleolar hypertrophy.

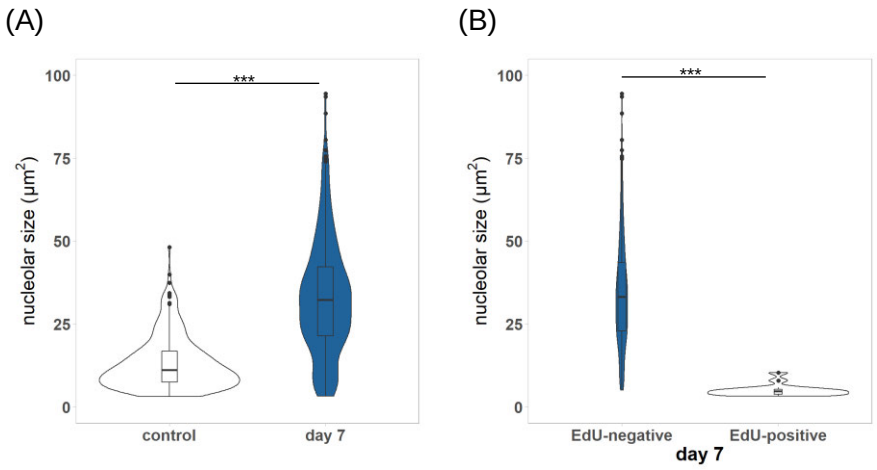

Figure 13: Inspection of nucleolar area between control and day 7 and between day 7 EdU-positive and day 7 EdU-negative ER:Ras IMR90. (A) Nucleolar area was found to be significantly escalated in day 7 ER:Ras IMR90 cells ($p<0.001$), suggesting OIS gave rise to nucleolar expansion. n=291 and 398 for control and day 7 respectively. (B) EdU-negative cells exhibited significantly enlarged nucleoli with an average size of 34.40μm^2 ($p<0.001$), compared to the size of nucleoli from EdU-positive cells. n=380 and 18 for EdU-negative and –positive respectively. Data from (A) and (B) were analysed by student's t-test.

3.3: Investigation of intracellular changes in oncogene-induced senescence

3.3.1: Nuclear area was significantly increased by oncogene-induced senescence

Following the examination of nucleolar area, other intracellular changes were investigated. I noticed nuclear size seemed to be changed during OIS while observing cells via microscopy. Therefore, I decided to examine nuclear area. Nuclear area was measured and quantified by CellProfiler and ImageJ as described in Methods and Materials. First of all, difference in nuclear area between control and day 7 ER:Ras IMR90 was examined. Automated image analysis by both CellProfiler and ImageJ identified a significant increase in nuclear area in day 7 cells ($p<0.001$), suggesting that, along with nucleolar

expansion, nuclear area was also enlarged by OIS (Figure 14A and B). Hence, oncogenic stress caused alterations in nuclear area.

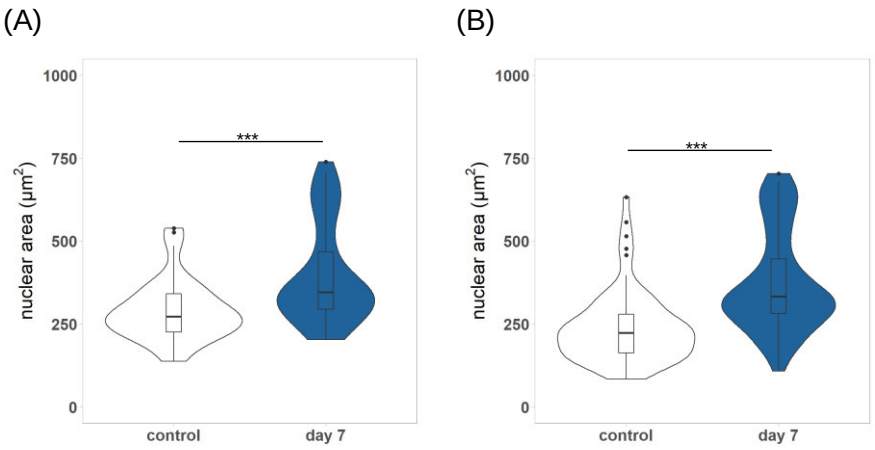

Figure 14: Nuclear area became significantly greater during OIS. (A and B) Upon 4-OHT incubation for 7 days, nuclear area was significantly increased ($p<0.001$). This proposes OIS caused expansion in nuclear area. Student's t-test was performed to analyse the data. (A) n=36 and 48 for control and day 7. (B) n=66 and 61 for control and day 7.

Next, nuclear area was analysed in the time-course of OIS. Using CellProfiler and ImageJ respectively, nuclear area was measured and quantitated. The time-course experiment revealed a significant increase in nuclear area from day 2 ($p<0.01$) although there was a wide variation in nuclear area within cells of the same day (Figure 15 A and B). The result indicates changes in nuclear area seem to occur rapidly, probably before or around day 2 when cells were affected by oncogenic stimuli. Supporting the results, investigation of nuclear area using external images (i.e. Col and Jag images, described in Methods and Materials) showed enlarged nuclear area was accompanied by the establishment of OIS (data not shown). Together, the time-course experiment suggests nuclear area becomes significantly enlarged by OIS.

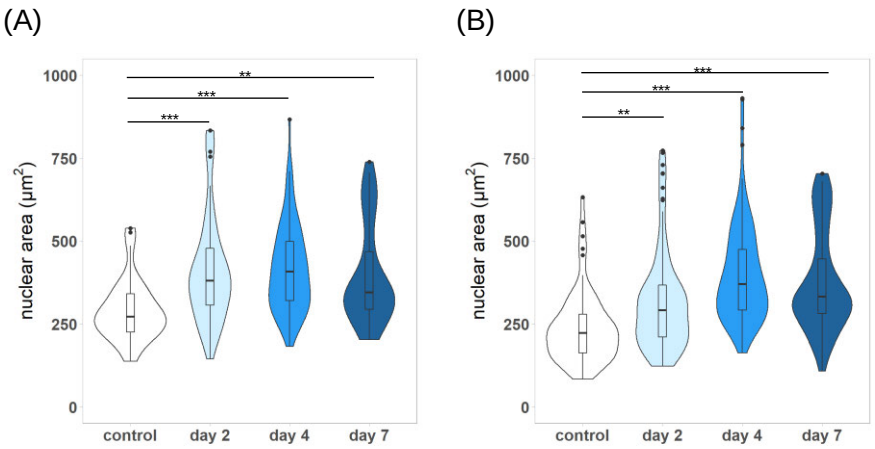

Figure 15: A significant increase in nuclear area was caused by OIS. (A and B) Time-course experiment identified nuclear area was significantly enlarged in OIS-induced ER:Ras IMR90 ($p<0.01$). Furthermore, changes in nuclear size seemed to appear at an early timepoint of OIS. All data were analysed by one-way ANOVA followed by a post-hoc Tukey's HSD correction. (A) n=36, 63, 81, and 48 for control, day 2, 4, and 7 respectively. (B) n=66, 101, 111, and 61 for control, day 2, 4, and 7 respectively.

3.3.2: Association between nucleolar hypertrophy and SAHF formation in oncogene-induced senescence

3.3.2.1: Introduction

Senescence-associated heterochromatin foci (SAHF) refer to a rearranged heterochromatin structure, which can be displayed as conglomerated foci when stained with DAPI (Chandra et al., 2012; Narita et al., 2003) (Figure 16). Each focus represents one chromosome and it is composed of multiple distinct layers of chromatin structure such as constitutive heterochromatin and facultative heterochromatin identified by H3K9me3 and H3K27me3 antibodies respectively. These transcriptionally repressive layers are separated from euchromatic regions found at the outer layer of SAHF (Chandra et al., 2012; Zhang et al., 2007). SAHF formation is not an absolute nuclear phenotype in OIS-induced cells because about 70% of OIS-induced cells exhibited SAHF formation (Teo et al., 2019). However,

cells that have established secondary senescence or RS reveal SAHF-negative features in a high proportion of the population, which contrasts with an enriched SAHF-positive characteristic in OIS (Kosar et al., 2011; Parry et al., 2018; Teo et al., 2019). There are some studies which show key regulators of SAHF formation, including DNA methyltransferase 1 (DNMT1) and High-Mobility Group A (HMGA) (Narita et al., 2006; Sati et al., 2020), yet the foundation of SAHF formation is not well understood. Similarly, the functions of SAHF are rather unclear, although SAHF were initially thought to contribute to gene regulation, in particular towards maintaining cellular senescence by silencing gene expression linked with proliferation (Narita et al., 2003; Zhang et al., 2007). Besides, despite the link between OIS and SAHF formation, it is not elucidated whether SAHF formation is associated with nucleolar expansion in OIS. Therefore, I decided to inspect the link between nucleolar hypertrophy and SAHF formation in OIS.

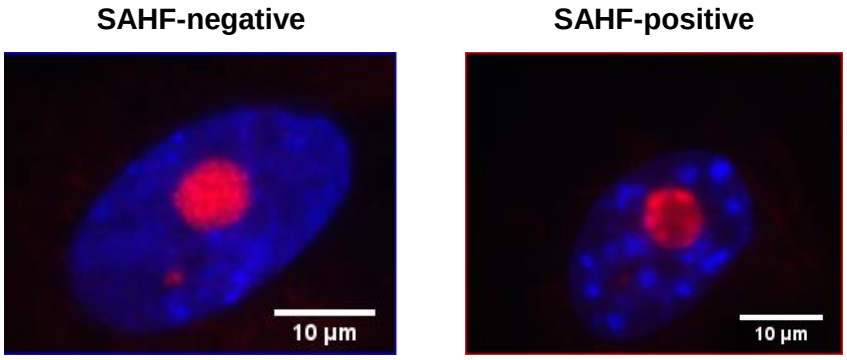

Figure 16: Images of SAHF-negative and –positive ER:Ras IMR90. Nucleus and nucleolus were stained by DAPI and fibrillarin antibody (ab4566, Abcam) with secondary antibody (Alexa Flour® 555). While the SAHF-negative cell showed smooth DAPI staining, the SAHF-positive cell exhibited spotty DAPI staining. The cells were visualised by epifluorescent microscopy with x40 magnification.

3.3.2.2: Nucleolar hypertrophy may associate with SAHF formation

In order to assess the link between nucleolar expansion and SAHF formation during OIS, images of cells stained by anti-fibrillarin were separated into two groups, SAHF-negative and SAHF-positive, and nucleolar area was examined by both CellProfiler and ImageJ. Subsequently, nucleolar size was compared between day 7 SAHF-negative and –positive ER:Ras IMR90. Nucleolar area quantified by CellProfiler conferred no difference (p=0.085) although the mean of nucleolar area was increased from 42.24μm^2 to 55.73μm^2 (Figure 17A). By contrast, nucleolar area measured by ImageJ identified a significant increase in nucleolar area in SAHF-positive cells with an average size of 44.50μm^2 compared to nucleolar area identified in SAHF-negative cells whose nucleolar area was 26.17μm^2 on average (p=0.007) (Figure 17B). A possible explanation for these inconsistent results may be the small sample size, particularly of day 7 SAHF-negative cells (n=7 and n=9). The low abundance of day 7 SAHF-negative cells was likely due to the length of 4-OHT incubation time that was sufficient to develop OIS and subsequently SAHF formation. Therefore, it was difficult to obtain a sufficient number of samples for day 7 SAHF-negative cells.

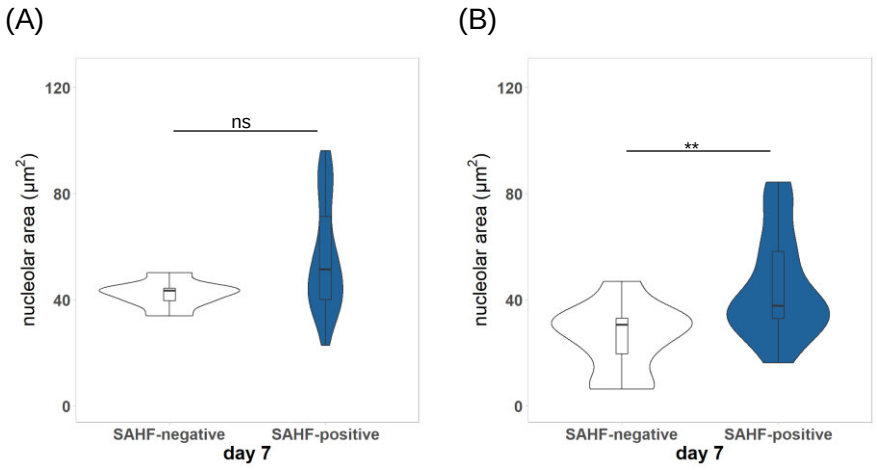

Figure 17: Nucleolar area comparison between day 7 SAHF-negative and day 7 SAHF-positive cells in OIS. (A and B) Although the mean nucleolar

area was generally increased in SAHF-positive cells, there were dissimilar results. The lack of day 7 SAHF-negative samples restricted the investigation of the link between nucleolar expansion and SAHF formation in OIS. Student's t-test was utilised for analysis. (A) n=7 and 43 for SAHF-negative and –positive. (B) n=9 and 43 for SAHF-negative and –positive.

Differences in nucleolar area between SAHF-negative and SAHF-positive cells was also investigated by ImageJ using images from external sources. Similar to previous outcomes, the analysis revealed rather contradictory results, uncovering both significantly increased nucleolar area in SAHF-positive cells and no difference (p=0.032 and p=0.106 respectively) (Figure 18A and B). The average size of nucleoli identified from SAHF-positive cells was about 49µm^2 in both analyses, which was approximately increased by 10µm^2 to 15µm^2 compared to SAHF-negative cells (Figure 18A and B). However, there were small numbers of SAHF-negative cells (n=27 and n=6) used for analysis. Taken together, these results from immunofluorescence image analysis need to be interpreted with caution and it was not possible to accept or rule out the link between nucleolar hypertrophy and SAHF formation in OIS. Multiple experimental replicates are required to collect sufficient number of cells, in particular day 7 SAHF-negative cells, to validate the outcome.

(A)

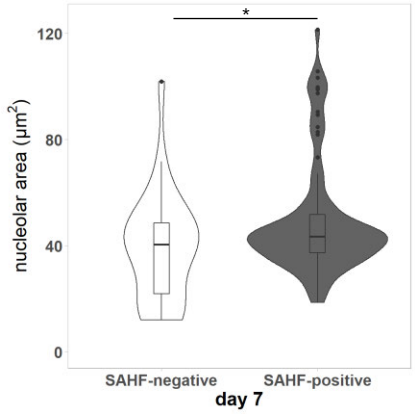

(B)

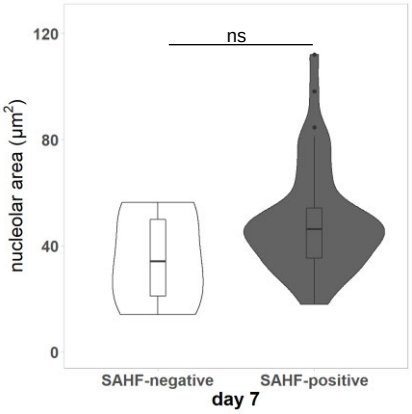

Figure 18: Nucleolar size comparison between day 7 SAHF-negative and day 7 SAHF-positive ER:Ras IMR90. (A and B) Generally, there was increased nucleolar area on average in SAHF-positive cells. However, the results from analyses were not consistent. All data were analysed by student's t-test. (A) n=27 and 89 for SAHF-negative and -positive. (B) n=6 and 45 for SAHF-negative and –positive.

Given that the inconsistent results were returned throughout the analysis on the link between nucleolar expansion and SAHF formation, I decided to further investigate the association. As previously explained, immunofluorescence images did not enable proliferative or senescent cells to be distinguished from the population of cells, especially in SAHF-negative cell populations (Figure 19A). This led to the possibility that the SAHF-negative cells in which nucleolar area had been previously analysed included both growing and OIS-induced cells rather than OIS-induced cells alone. The proliferative cells need to be eliminated from the SAHF-negative cell population to purify OIS-induced cells and this will likely enhances the accuracy of analysing the link between nucleolar hypertrophy and SAHF formation within the OIS-induced cell population. To remove growing cells, ER:Ras IMR90 images from the EdU assay were used for analysis since they allow the exclusion of EdU-incorporated cells that certainly correspond to proliferative cells (Figure 19B). Nucleolar area was measured and quantitated by ImageJ in day 7 EdU-negative SAHF-negative and day 7 EdU-negative SAHF–positive cells. As a consequence of this analysis, significantly increased nucleolar size was determined in SAHF-positive cells ($p<0.001$) (Figure 20). The result possibly proposes that nucleolar hypertrophy is linked with SAHF formation during OIS although further investigation is required.

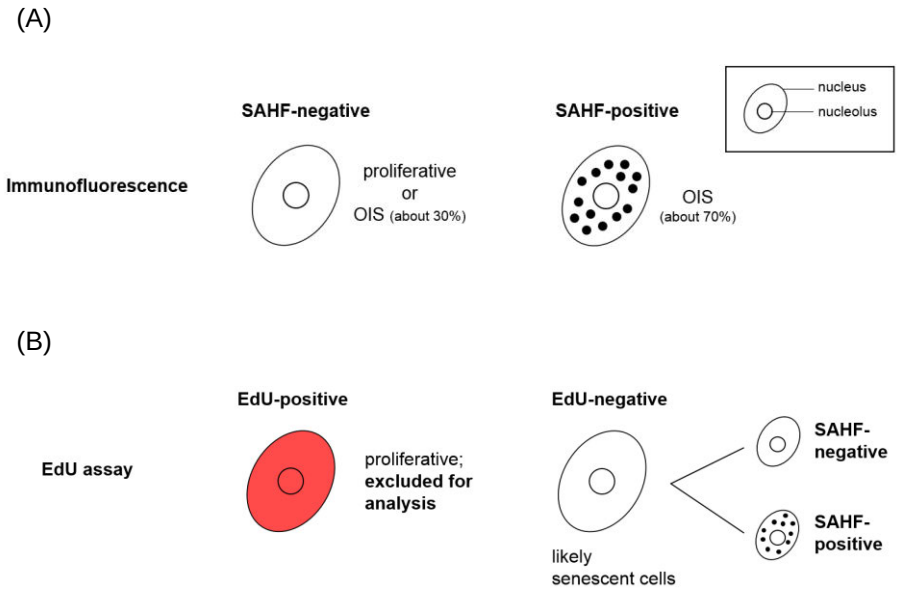

Figure 19: A schematic diagram of immunofluorescently-stained and EdU-stained ER:Ras IMR90 cells. (A) SAHF-negative cell images from immunofluorescence include both proliferative and OIS-induced cells. It was not possible to distinguish senescent cells from proliferative cells in an immunofluorescence setting. (B) Cell images from the EdU assay allowed for the removal of proliferative cells by excluding EdU-incorporated cells. This increased the chance of analysing nucleolar area only in senescent cells.

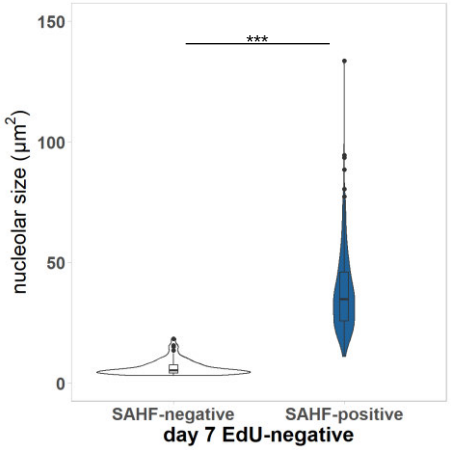

Figure 20: Nucleolar expansion seems to associate with SAHF formation in OIS. The images of day 7 EdU-negative cells were divided into two groups based on SAHF formation and nucleolar area was measured by ImageJ. Nucleolar area was significantly escalated in SAHF-positive cells ($p<0.001$) with the average size of 37.82μm^2, likely indicating that nucleolar hypertrophy

links with SAHF formation during OIS. Student's t-test was used for analysis. n=71 and n=326 for SAHF-negative and –positive cells respectively.

3.4: Examination of gene expression associated with alterations in nucleoli during oncogene-induced senescence

3.4.1: Introduction

RNA sequencing (RNA-seq) is a technique that allows the examination of the whole transcriptome using next-generation sequencing technology. RNA-seq gives information on changes in gene expression between two or more samples, thereby being used for differential gene expression analysis.

To understand gene expression associated with enlarged nucleoli in OIS and RS, I was originally planning to divide cells according to the size of nucleolus within the cell populations of control, OIS, and RS and perform RNA-seq. However, due to COVID-19, the planned experiment was replaced. Instead, I investigated genes associated with nucleolar area, structure, or morphology from peer-reviewed journals (Table 9), which were utilised for RNA-seq analysis afterwards. In essence, 15 genes were found to have a relationship with nucleolar alterations. Firstly, the depletion of genes encoding nucleolar proteins including fibrillarin (FBL), nucleolin (NCL), and UBF resulted in nucleolar disruption (Hayashi et al., 2018; Tiku et al., 2017; Ugrinova et al., 2007). MYBBP1A was included since it is an enriched nucleolar protein, used as a nucleolar marker, and plays an important role in p53 activation under nucleolar stress (Kumazawa et al., 2015) despite no evidence showing nucleolar distortion upon the knockdown of the gene. The knockdown of other nucleolar protein genes such as nucleolar protein 11 and 12 (NOL11 and NOL12 respectively) led to aberrant nucleolar area or morphology (Freed et al., 2012; Hayashi et al., 2018; Pinho et al., 2019). Interestingly, NOL12 expression level was reported to decrease with normative aging (Pinho et al., 2019). NOL11 is essential for optimal rDNA transcription and pre-rRNA processing (Freed et al., 2012). Secondly, the inactivation of the RPL5, RPL11,

and RPL15 genes induced the loss of nucleolar structure maintenance (Dong et al., 2019; Nicolas et al., 2016). These ribosomal protein genes generate gene products that are components of 60S ribosomal proteins, thereby being crucial for ribosome biogenesis. Thirdly, upon the knockout of lamin A, B1, B2 and SUN1 genes, nucleolar morphology was distorted (Buchwalter and Hetzer, 2017; Gupta and Sengupta, 2017; Martin et al., 2009; Matsumoto et al., 2016). Lamin proteins and SUN1 primarily function as architectural proteins of the nuclear membrane. Notably, Hutchinson-Gilford progeria syndrome (HGPS) caused by mutation in the lamin A gene (mutant lamin A is termed as progerin) results in nucleolar expansion and upregulated ribosome biogenesis (Buchwalter and Hetzer, 2017). Lastly, the disruption of other genes such as RRN3 and juxtaposed with another zinc finger protein 1 (JAZF1) were determined to trigger changes in nucleolar area or morphology (Chen et al., 2018; Kobiita et al., 2020). RRN3 encodes TIF-IA which is crucial for the initiation of rDNA transcription by tethering RNA polymerase I (Chen et al., 2018). JAZF1 was recently shown to have a role in rRNA processing and the transcription of ribosomal proteins (Kobiita et al., 2020).

Gene	Functions of protein	Reference
FBL	methyltransferase (methylate histone H2A), rRNA processing	Tiku et al., 2017
NCL	pre-rRNA processing and maturation	Ugrinova et al., 2007
MYBBP1A	rDNA transcription regulator	Enriched proteins in nucleoli (no reference)
UBF	rDNA transcription factor	Hayashi et al., 2018
NOL11	rDNA transcription and pre-rRNA processing	Freed et al., 2012; Hayashi et al., 2018
NOL12	pre-rRNA processing	Pinho et al., 2019
RPL5	ribosome biogenesis	Nicolas et al., 2016

RPL11	ribosome biogenesis, rRNA processing	Nicolas et al., 2016
RPL15	ribosome biogenesis, pre-rRNA processing	Dong et al., 2019
LMNA	nuclear structure integrity	Buchwalter and Hetzer, 2017
LMNB1	nuclear structure integrity	Martin et al., 2009
LMNB2	nuclear structure integrity	Gupta and Sengupta, 2017
SUN1	nuclear maintenance	Matsumoto et al., 2016
RRN3	rDNA transcription factor	Chen et al., 2018
JAZF1	rRNA processing, ribosomal protein gene regulator	Kobiita et al., 2020

Table 9: The list of genes associated with nucleolar area, structure, or morphology. The references cited in this table have evidenced nucleolar area, structure, or morphology was disrupted upon the depletion of these genes.

3.4.2: Ribosomal protein genes and RRN3 were upregulated, yet JAZF1, nucleolar protein genes and lamin protein genes were downregulated in oncogene-induced senescence

Subsequent to the gene search from peer-reviewed papers, I used RNA-seq data from the research group of Dr. Peter. D Adams (Rai et al., 2014). Quality control, trimming, and read alignment was performed by Neil Robertson from Dr. Tamir Chandra's research group. The SeqMonk software was employed to quantitate the processed RNA-seq data as described in Methods and Materials. The genes shown in Table 9 were used as probes to determine gene expression linked with nucleolar alterations in OIS. The result of RNA-seq analysis showed that ribosomal protein-encoding genes and RRN3 were upregulated in OIS (Figure 21). In contrast, JAZF1, lamin protein-encoding genes, and nucleolar protein-encoding genes were suppressed in OIS (Figure 21). Such gene expression features likely relate to the accelerated rRNA transcription and abnormal ribosome biogenesis found in OIS, which

are in turn connected to increased nucleolar size. Taken together, the RNA-seq analysis results indicate the enlarged nucleolar area in OIS was likely orchestrated by the upregulation of ribosomal protein genes and TIF-IA transcription factor genes and the downregulation of lamin protein genes, nucleolar protein genes, and JAZF1. Importantly, the effects of other signals and genes that are related to nucleolar alterations yet excluded from this analysis cannot be discounted.

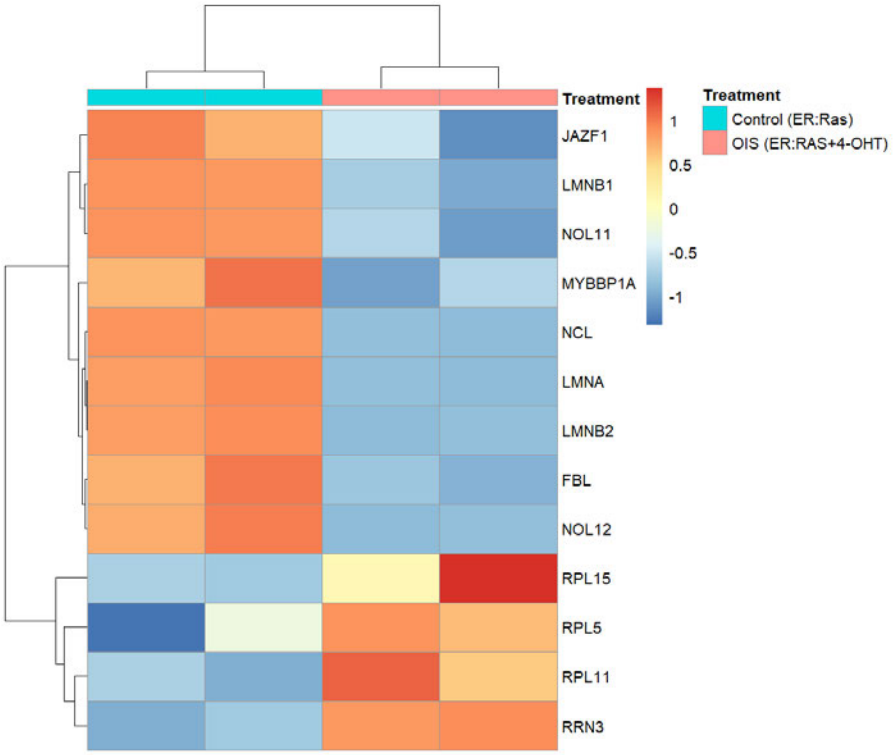

Figure 21: RNA-seq analysis of genes linked with nucleolar alterations in OIS. OIS-induced IMR90 cells overexpressed ribosomal protein genes including RPL5, RPL11, and RPL15 and a transcription factor gene, RRN3. By contrast, nucleolar protein- and lamin protein-encoding genes and JAZF1 were downregulated in OIS.

Chapter IV

Nucleolar Dynamics in Secondary Senescence

4.1: Secondary senescence was triggered by cell-cell interaction

To examine the nucleolar dynamics in secondary senescence, the co-culture system was employed as described in Materials and Methods (Figure 4). Following the co-culture of cells, the co-cultured cells were incubated with 4-OHT for different time period such as two, four, or seven days (referred to as day 2, 4, or 7 cells respectively). mVenus:EV cells without 4-OHT treatment was used as control. Unlike the ER:Ras IMR90 cells, mVenus:EV cells did not exhibit the ER:Ras construct, and thereby did not establish OIS. Instead, mVenus:EV could develop secondary senescence via cell-cell communication (for example, SASP and Notch signalling) between mVenus:EV and OIS-induced ER:Ras IMR90.

Firstly, the development of secondary senescence in mVenus:EV cells was investigated by EdU assay (Figure 5A). 12 hours of EdU incubation was utilised to improve the identification of senescent mVenus:EV cells; the prevalence of EdU-positive cells was compared between control and day 7 mVenus:EV. A significantly attenuated proliferation rate was recognised in day 7 mVenus:EV ($p=0.02$) (Figure 22). This suggests the co-cultured OIS-induced ER:Ras IMR90 contributed to the development of secondary senescence in mVenus:EV. Unlike OIS triggered by Ras overexpression in ER:Ras IMR90, it was not easy to pinpoint the main contributors towards the establishment of secondary senescence in mVenus:EV. Nevertheless, other studies also supported secondary senescence being induced in a paracrine manner through SASP or a juxtacrine manner via Notch signalling (Hoare et al., 2016; Parry et al., 2018; Teo et al., 2019). Hence, secondary senescence was established in day 7 mVenus:EV by cell-cell communication between OIS-induced ER:Ras IMR90 and mVenus:EV. Notably, there was an outstanding difference identified between day 7 ER:Ras IMR90 and day 7 mVenus:EV in the images

from EdU assay. While the population of day 7 ER:Ras IMR90 cells exhibited a higher level of DAPI intense foci, representing senescence-associated heterochromatin foci (SAHF), most day 7 mVenus:EV cells did not display such a chromosomal rearrangement.

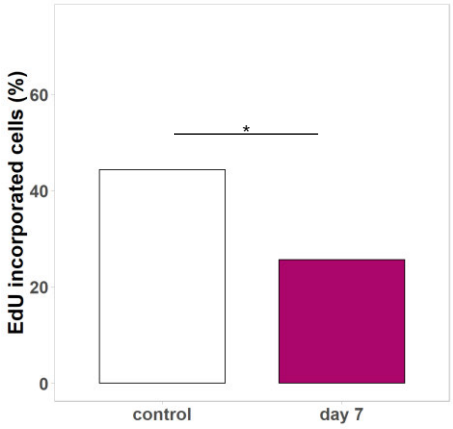

Figure 22: Secondary senescence was determined by EdU assay. There were significantly fewer EdU-incorporated cells in day 7 population than in the control population (p=0.02). The result indicates reduced proliferative capacity was due to the establishment of secondary senescence via cell-cell communication with OIS-induced ER:Ras IMR90. Student's t-test was performed to analyse the data. n=183 for EdU-incorporated cells (total number of cells = 413 cells) in control and n=109 for EdU-positive cells (total number of cells = 425 cells) in day 7.

4.2: Investigation of nucleolar area in secondary senescence

4.2.1. Nucleolar hypertrophy was not identified in secondary senescence

To start with, the difference in nucleolar area between control and day 7 mVenus:EV was investigated by immunofluorescence using an anti-fibrillarin antibody (ab4566, Abcam) with a goat anti mouse (Alexa Flour® 555) secondary antibody. Subsequent to immunofluorescence staining, nucleolar size was quantitated by CellProfiler and ImageJ (Figure 23). Surprisingly, nucleolar area was not significantly different between control and day 7 mVenus:EV cells (p>0.05) (Figure 24A).

Consistently, nucleolar area measured by ImageJ revealed no significant difference (p>0.05) (Figure 24B). The mean of nucleolar area was determined to be between 14μm^2 and 16μm^2 for control whereas it was 15μm^2 in day 7 mVenus:EV cells. Hence, secondary senescence did not give rise to nucleolar hypertrophy.

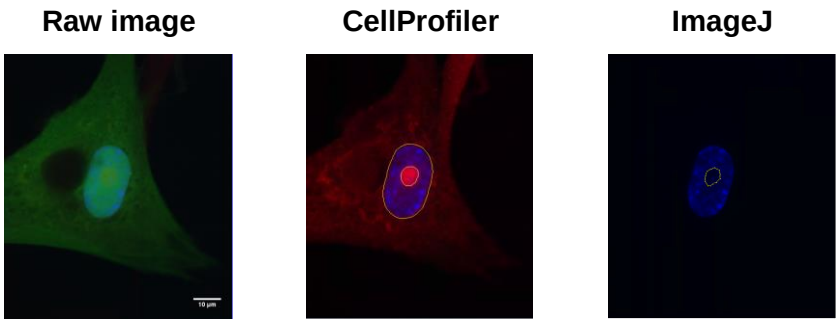

Figure 23: The measurement of nucleoli in mVenus:EV using CellProfiler and ImageJ. The raw immunofluorescence images of mVenus:EV were used for analysing nucleolar area by CellProfiler and ImageJ. CellProfiler was used to mark nucleoli and nuclei and subsequently quantified the area of them. Alternatively, ImageJ was employed to quantitate nucleolar and nuclear size. The DAPI-negative region was used to measure nucleolar area.

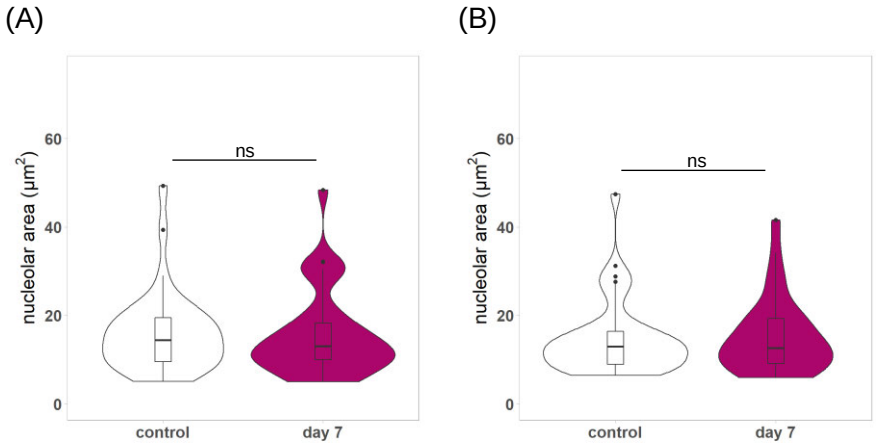

Figure 24: Nucleolar area was not significantly altered in day 7 mVenus:EV. (A and B) The examination of nucleolar area in control and day 7 mVenus:EV revealed no significant difference in nucleolar area (p>0.05), suggesting secondary senescence did not increase nucleolar size. Both sets

of data were analysed by student's t-test. (A) n=35 for both control and day 7 respectively. (B) n=37 and 30 for control and day 7 respectively.

After an investigation of the difference in nucleolar size between control and day 7 mVenus:EV, it was examined whether the lack of difference in nucleolar area could be observed during the course of secondary senescence. Therefore, alterations in nucleolar area were inspected by time-course experiment followed by automated image analysis. As expected, nucleolar area was not significantly different at any point throughout the time-course experiment ($p>0.05$) (Figure 25A and B). Despite the variance of nucleolar area within the same population of cells, the nucleolar size was within a limited range, generally between 10µm^2 and 50µm^2 throughout the time during which secondary senescence was established. This variation was much narrower than that found in OIS. The outcome from the time-course experiment supports the idea that secondary senescence does not trigger an increase in nucleolar size.

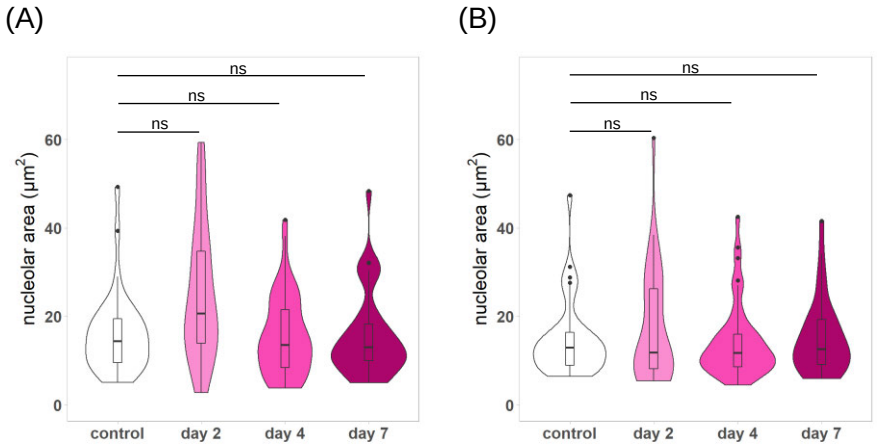

Figure 25: The examination of nucleolar area in the course of secondary senescence. (A and B) No significant change in nucleolar size was found throughout the timepoints ($p>0.05$), indicating secondary senescence did not cause nucleolar hypertrophy. One-way ANOVA was performed to analyse the data, which was followed by a post-hoc Tukey's HSD correction. (A) n=35, 22,

48, and 35 for control, day 2, 4, and 7 respectively. (B) n=37, 32, 45, and 30 for control, day 2, 4, and 7 respectively.

To further confirm no nucleolar hypertrophy occurred in the course of the cell developing secondary senescence, nucleolar area was investigated using external source images (described in section 2.5.4 in Methods and Materials). Consistent with previous results, nucleolar area was not significantly different between the control mVenus:EV and other days of mVenus:EV cells that were co-cultured with OIS-induced ER:Ras IMR90 ($p>0.05$) (Figure 26A and B). Therefore, these results propose secondary senescence did not trigger nucleolar expansion. Moreover, similar to the previous finding, nucleolar size varied from 10µm^2 to 50µm^2. The results from the time-course experiment uncovered rather striking differences when compared to the co-cultured ER:Ras IMR90. While mVenus:EV did not display enlarged nucleoli during secondary senescence (Figure 25 and 26), ER:Ras IMR90 showed nucleolar hypertrophy at an early time point of OIS development, probably earlier than or around day 4 (Figure 11 and 12). Such different nucleolar phenotypes likely suggest different senescence inducers caused distinct nucleolar stress.

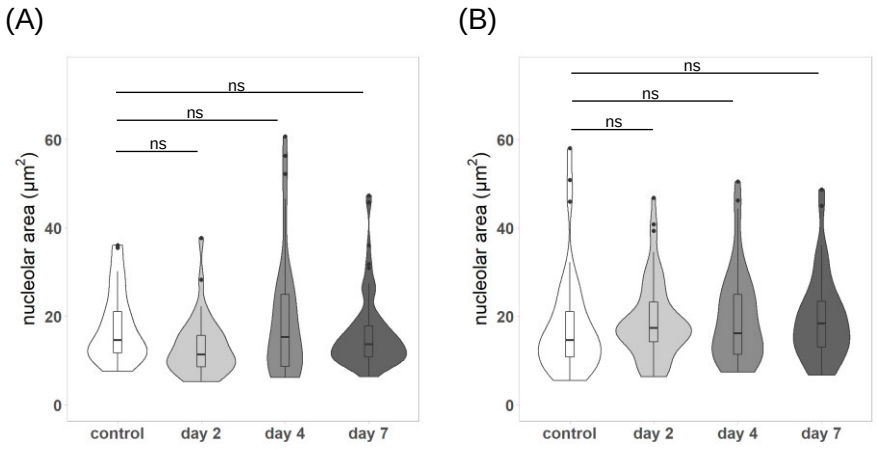

Figure 26: Nucleolar size was not altered throughout the time-course experiment. (A and B) There was no significant change in nucleolar size

during the process of secondary senescence establishment in mVenus:EV cells ($p>0.05$). The outcome indicates secondary senescence is unlikely to contribute to nucleolar expansion. The data was analysed by one-way ANOVA followed by a post-hoc Tukey's HSD correction. (A) n=40, 30, 41, and 80 for control, day 2, 4, and 7 respectively. (B) n=42, 55, 45, and 43 for control day 2, 4, and 7 respectively.

Lastly, images of mVenus:EV cells from an EdU assay were used for analysing nucleolar area in secondary senescence. As previously explained, the advantage of analysing nucleolar area using cell images from the EdU assay is to allow proliferative cells to be distinguished from the cell population. Therefore, there is the benefit of purifying two separated cell populations, growing and senescent cells, thereby improving the examination of nucleolar size in proliferative and senescent groups. ImageJ was utilised to quantitate the difference in nucleolar area between day 7 EdU-negative and –positive mVenus:EV. Although nucleolar size was identified to be significantly increased in day7 EdU-negative cells ($p=0.03$) (Figure 27A), the validity of the result was uncertain by a small number of day 7 EdU-positive mVenus:EV (n=26). Furthermore, the mean nucleolar area in day 7 EdU-negative and –positive mVenus:EV was different to a limited extent, 15μm^2 versus 11μm^2. This may suggest a few day 7 EdU-negative mVenus:EV cells exhibited much larger nucleoli (noted as outliers in Figure 27A) and they possibly contributed to a false positive outcome. Taken together, these results show that nucleolar area is unlikely enlarged by secondary senescence even though more replicates are required to confirm the nucleolar dynamics that occur during secondary senescence.

Finally, nucleolar area of cells was compared between OIS and secondary senescence using cell images from the EdU assay. There was a diverse nucleolar size within the day 7 EdU-negative ER:Ras IMR90 and mVenus:EV cell populations, yet the ER:Ras IMR90 showed much wider variation (Figure 27B). More interestingly, a significant difference in nucleolar area was determined between day 7 EdU-negative ER:Ras IMR90 and mVenus:EV ($p<0.001$) (Figure 27B).

OIS seemed to trigger severe nucleolar hypertrophy whereas the impact of secondary senescence on nucleoli was obscure. This likely proposes cell nucleoli respond differently to different senescence inducers and that these inducers possibly cause distinct nucleolar stress, as reflected by nucleolar size.

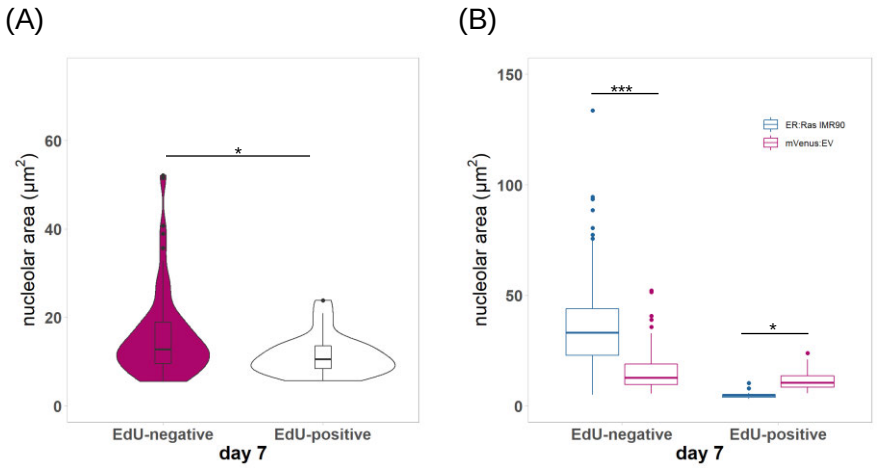

Figure 27: Secondary senescence did not trigger changes in nucleolar size whereas OIS induced nucleolar hypertrophy. (A) day 7 EdU-negative mVenus:EV were determined to exhibit enlarged nucleoli ($p=0.03$). Despite being statistically significant, a few day 7 EdU-negative mVenus:EV cells (shown as outliers) were thought to contribute to a false-positive result. The data was analysed by student's t-test. n=80 and 26 for EdU-negative and –positive cells. (B) There was disparity in nucleolar size between day 7 EdU-negative ER:Ras IMR90 and mVenus:EV ($p<0.001$), suggesting oncogenic stress cause considerable nucleolar expansion whereas the effect of secondary senescence was unclear. Although EdU-positive mVenus:EV cells showed significantly different nucleolar area when compared to EdU-positive ER:Ras IMR90 ($p<0.05$), it was probably due to the diverse size of nucleoli present in growing cells. Student's t-test was used for data analysis. n=381 and 80 for day 7 EdU-negative ER:Ras IMR90 and mVenus:EV respectively. n=18 and 26 for day 7 EdU-positive ER:Ras IMR90 and mVenus:EV respectively.

4.3: Examination of intracellular changes in secondary senescence

4.3.1. Secondary senescence did not cause changes in nuclear area and SAHF formation

Following the analysis of nucleolar area, I started investigating intracellular changes caused by secondary senescence. Firstly, nuclear size was examined in secondary senescence. CellProfiler and ImageJ were used for measuring and quantifying nuclear area between control and day 7 mVenus:EV. Although there was greater variation in nuclear size in day 7 mVenus:EV than the control, no significant change in nuclear area was determined when compared to the control ($p>0.05$) (Figure 28A). Similarly, the analysis using ImageJ showed nuclear area was not significantly different between control and day 7 mVenus:EV (Figure 28B). Corresponding to these outcomes, the analysis of nuclear area using images from the EdU assay did not find a significant difference in nuclear area between control and day 7 mVenus:EV (data not shown). Taken together, the results suggest secondary senescence did not alter nuclear area.

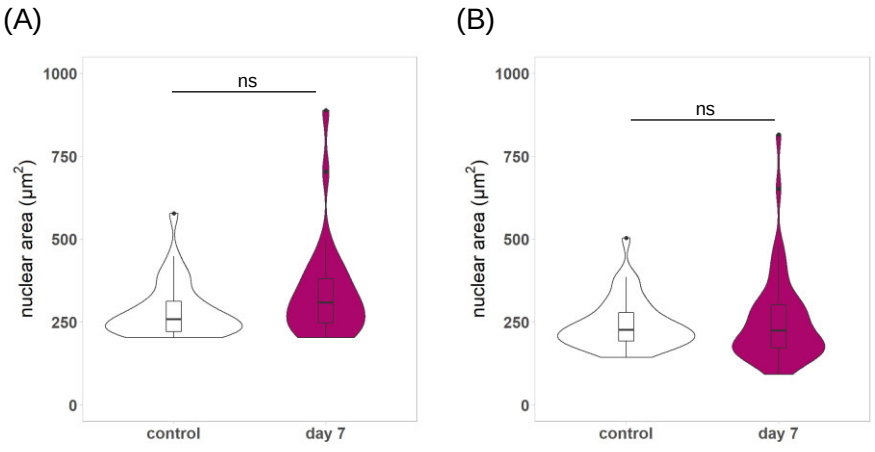

Figure 28: Nuclear area was not significantly changed by secondary senescence. (A and B) Nuclear size was not significantly changed in day 7 mVenus:EV ($p>0.05$), indicating secondary senescence did not result in an alteration in nuclear size. All data were analysed by student's t-test. (A) n=32

and 28 for control and day 7 cells respectively. (B) n=38 and 44 for control and day 7 cells respectively.

To further confirm that nuclear area was unaffected by secondary senescence, I examined the dynamics of nuclear area during the course of secondary senescence using a time-course experiment. Nuclear size was quantitated by CellProfiler and ImageJ. As expected, analysis by CellProfiler identified the similarity between the nuclear area of the control and cell populations of incubation time ($p>0.05$) (Figure 29A). Likewise, nuclear area measured by ImageJ found no significant alterations in nuclear size throughout the time-course experiment ($p>0.05$) (Figure 29B). Hence, the results confirmed secondary senescence did not induce changes in nuclear area.

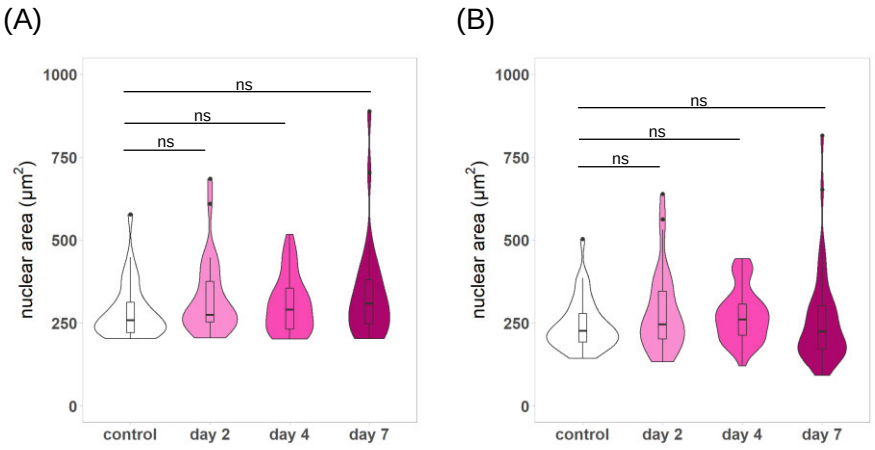

Figure 29: The examination of nuclear size in the course of secondary senescence. (A and B) There was no significant change in nuclear area throughout the time-course experiment ($p>0.05$), proposing secondary senescence did not cause a significant increase in nuclear size. One-way ANOVA was used for data analysis, followed by a post-hoc Tukey's HSD correction. (A) n=32, 29, 41 and 28 for control, day 2, 4, and 7 respectively. (B) n=38, 33, 45, and 44 for control, day 2, 4, and 7 respectively.

Lastly, SAHF formation was examined in day 7 mVenus:EV. As previously mentioned, one noticeable observation from the images

from the EdU assay was that mVenus:EV cells were a lack of SAHF formation compared to ER:Ras IMR90 cells. Indeed, 2% of mVenus:EV cells were identified to be SAHF-positive (6 out of 255 mVenus:EV cells), which was substantially lower than the prevalence of SAHF formation determined in OIS (on average 70% of cells in OIS were SAHF-positive). This suggests secondary senescence is unlikely to trigger SAHF formation.

Chapter V

Nucleolar Dynamics in Replicative Senescence

5.1: Long-term serial passage induced replicative senescence

To investigate the nucleolar dynamics during replicative senescence (RS), replicative stress was triggered by long-term serial passage using IMR90 human fibroblasts. As somatic cells have a replicative lifespan due to telomere shortening, prolonged cell passage allows the cells to develop RS. To determine whether RS was developed by long-term serial passage, the number of cells was measured by Countess II automated cell counter just before the cells were passaged. Then, accumulated cell counts were calculated as described in Materials and Methods. When somatic cells become replicatively senescent, the total number of cells tend to slowly increase, reflected as a plateau in accumulated cell counts over cell culture period. The early-passage IMR90 human fibroblasts showed a rapid growth of accumulated cell counts while the accumulated cell counts in late-passage cells were inclined to steadily rise (Figure 30). This result suggests the number of cells involved in DNA replication were reduced when cells repeatedly proliferated, indicating that the late-passage IMR90 human fibroblasts established RS by prolonged serial passage. Notably, only seven passages, instead of 10 passages, of accumulated cell counts were plotted as the stability and the state of balance in cells were disrupted by unavoidable freezing and thawing steps in the midst of the research project. To ensure the recovery of cell stability, cells were passaged three times upon reaching 80% confluency following thawing and they were subsequently used for further experiments including an EdU assay and immunofluorescence.

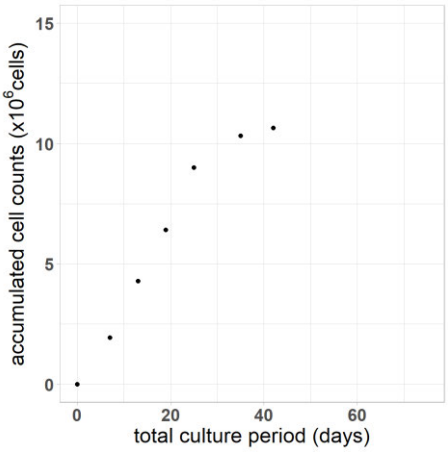

Figure 30: Prolonged culture of IMR90 human fibroblasts induced RS. The accumulated cell counts sharply increased in early-passage cells, proposing cells were actively replicated. However, the more times cells were passaged, the slower the accumulated cell counts grew, indicating a reduced number of proliferative cells. Hence, RS was triggered by long-term serial passage.

To further confirm the exhibition of RS in the late passage IMR90 human fibroblasts, cells were treated with 5-ethynyl-2′-deoxyuridine (EdU) for 12 hours (Figure 31A). EdU incorporation rate was monitored and compared between early-passage and late-passage IMR90 human fibroblasts (referred to as P17 and P24 respectively). Almost one third of early-passage cells incorporated EdU whereas only 2.5% of late-passage cells were found to be EdU-positive, suggesting the amount of EdU incorporation was significantly decreased ($p<0.001$) (Figure 31B). The EdU assay result indicates continuous serial passage caused RS in late-passage IMR90 human fibroblasts, corresponding to the outcome from accumulated cell counts. Notably, the observation of cell images from the EdU assay led to the discovery of very low levels of SAHF formation in late-passage cells. This seems to be a feature of nuclear phenotype shared by cells which have developed secondary senescence, yet it is contrast with OIS.

(A)

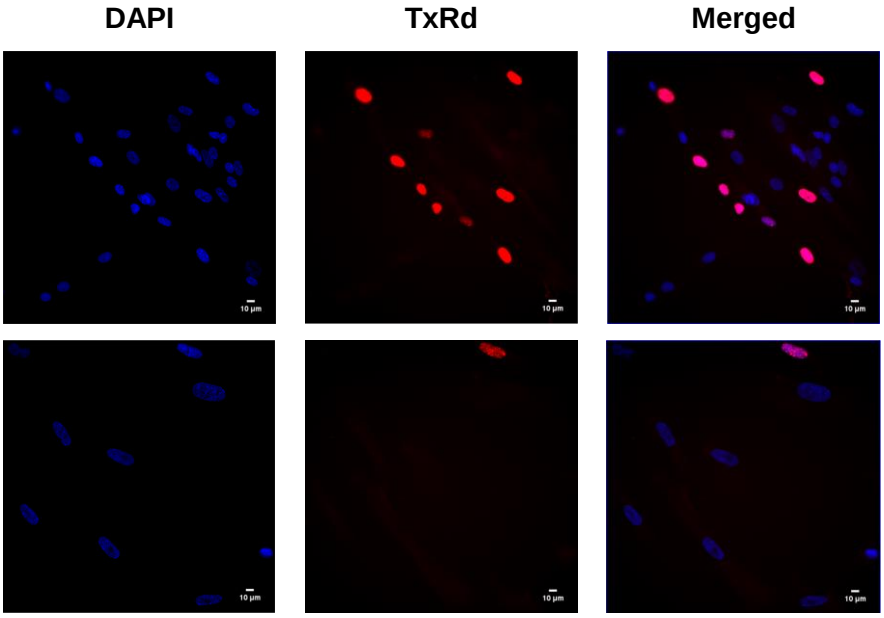

(B)

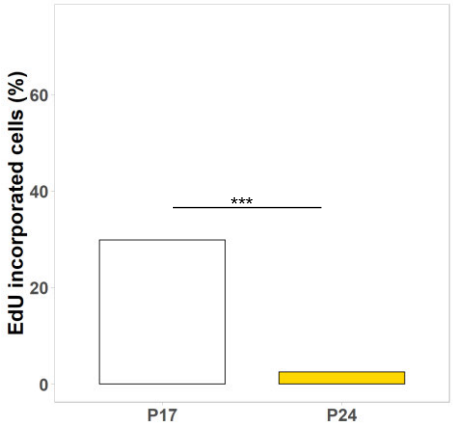

Figure 31: EdU incorporation assay of IMR90 human fibroblasts. (A) An EdU assay was performed on early- and late-passage IMR90 human fibroblasts. The top three images are early-passage cells (i.e. P17) and the bottom three images are late-passage cells (i.e. P24). Scale bar is 10μm. (B) An EdU incorporation rate was significantly reduced in P24, suggesting serial passaging triggered RS in late-passage IMR90 fibroblasts. Data was analysed by student's t-test. n=692 for EdU-positive cells (total number of cells = 2317 cells) in P17 and n=16 for EdU-incorporated cells (total number of cells = 646 cells) in P24.

5.2: Inspection of nucleolar area in replicative senescence

5.2.1: Optimisation of antibody concentration for immuno-fluorescence

Following the confirmation of RS in late-passage IMR90 human fibroblasts, nucleolar size was evaluated in P17 and P24 by immunofluorescence. Prior to immunofluorescence, the dose of anti-fibrillarin antibody (ab184817, Abcam) for immunofluorescence was optimised. Four different dilution factors were used as described in Materials and Methods (Table 4), and cells were visualised by epi-fluorescent microscope. The images showed clear nucleoli staining when cells were stained with 1:50 dilution of fibrillarin antibody (Figure 32). By contrast, nucleoli stained with a lower dilution of antibody were weakly visualised, especially when 1:200 and 1:400 dilutions of antibody were used (Figure 32). This was due to the low abundance of antibody attached to the nucleolar protein fibrillarin. Hence, the optimisation result indicates a 1:50 dilution of antibody was ideal for immunofluorescence.

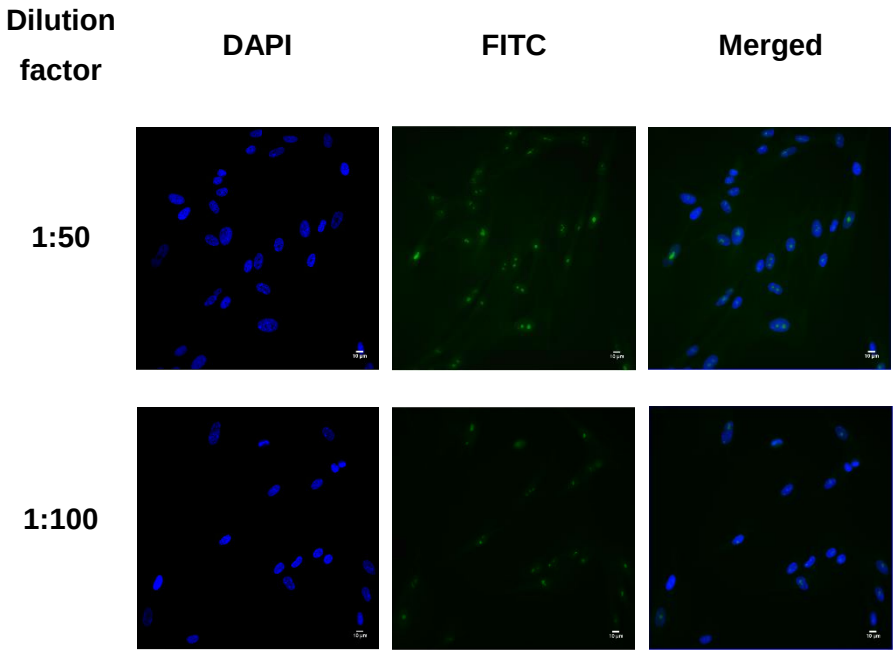

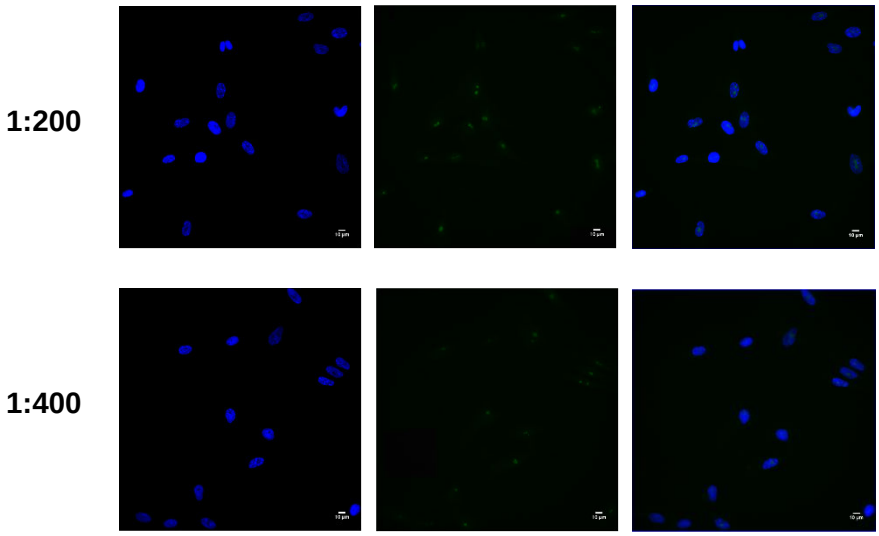

Figure 32: Antibody dose optimisation for immunofluorescence. IMR90 human fibroblasts were stained with a 1:50, 1:100, 1:200, and 1:400 dilution of anti-fibrillarin antibody respectively. Scale bar is 10µm.

5.2.2: Nucleolar area was significantly increased by replicative senescence

To investigate changes in nucleolar area by RS, cells were subjected to immunofluorescence staining by using two different antibodies, both of which specifically bind to nucleolar protein fibrillarin (Figure 33A and 35A). Subsequent to immunofluorescence staining, nucleolar and nuclear area were quantitated by CellProfiler (Figure 33B). Firstly, based on the observation of cell images from immunofluorescence, it seemed the size of nucleoli and nuclei were generally increased in P24 compared to P17 (Figure 33A). In spite of heterogeneous nucleolar area being determined within the populations of P17 and P24, the analysis of nucleolar area by CellProfiler uncovered a significant enlargement of nucleolar size in late-passage IMR90 human fibroblasts ($p<0.001$) (Figure 34A). The mean nucleolar size was 14.66µm^2 in P24 while it was 9.43µm^2 in P17. Hence, this suggests nucleolar area was increased by RS. One interesting finding was, despite there being nucleolar enlargement in RS, nucleolar expansion did not seem to be as severe as that which was identified in OIS. In

addition, the range of variation in nucleolar size was smaller in RS compared to the variation found in OIS. More specifically, the nucleolar area in RS did not generally expand beyond 70μm^2 while there were some OIS-induced cells whose nucleoli became enlarged beyond 70μm^2 (Figure 9, 11-13, and 34A). It is feasible to speculate that there would be shared as well as distinct mechanisms of establishing nucleolar hypertrophy between RS and OIS.

The increased nucleolar size in P24 led to a question: did small nucleoli in P17 merge together to form a large nucleolus or nucleoli in late-passage cells. This question was indirectly examined by counting the number of nucleolus per nucleus. Intriguingly, the late-passage cells tended to have a smaller number of nucleolus per nucleus (Figure 34B). About half of P17 exhibited one nucleolus and the rest of it contained more than one nucleolus per nucleus. In contrast to P17, nearly three quarters of P24 were determined to have one nucleolus, which was an increase of approximately 25%. This outcome indicates the number of nucleolus per nucleus was decreased by RS. The reduced number of nucleolus per nucleus in late passage cells may indicate a possibility that several small nucleoli could be integrated into each other, producing a nucleolus or nucleoli of greater size during RS, yet appropriate experiments are required to substantiate this hypothesis.

(A)

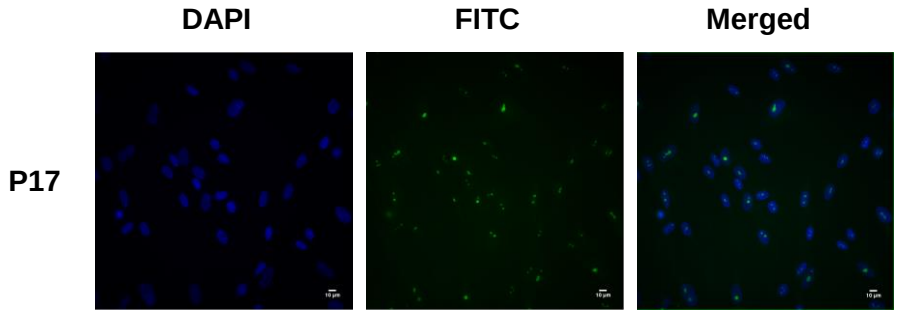

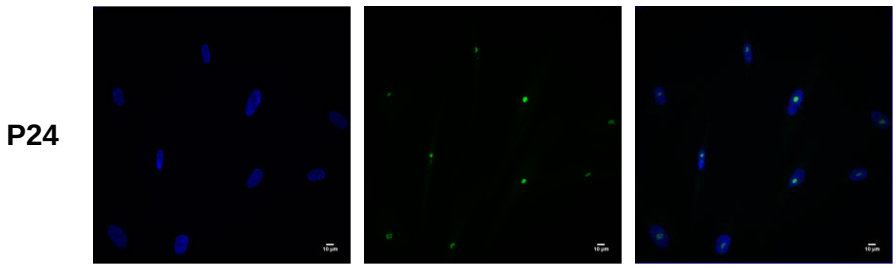

(B)

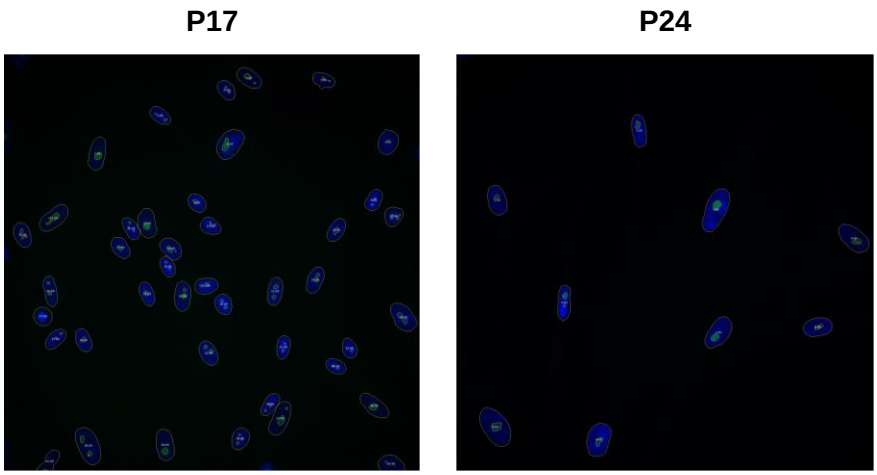

Figure 33: Immunofluorescence staining of IMR90 human fibroblasts and nucleolar size quantification by CellProfiler. (A) Fibrillarin antibody (ab184817, Abcam) and DAPI were utilised to stain nucleoli and nuclei respectively. An epifluorescent microscope with x40 magnification was employed to visualise the cells. The scale bar is 10µm. (B) CellProfiler was employed to quantitate nucleolar and nuclear size. A number was given to each nucleus, which allowed the tracking of the origin of the nucleoli from different nuclei.

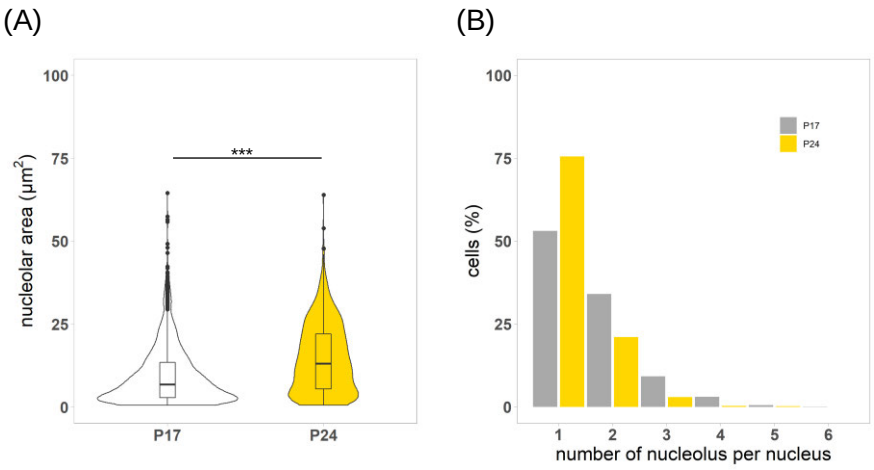

Figure 34: The examination of nucleolar area and the number of nucleolus per nucleus in RS. (A) A significant increase in nucleolar area was identified in P24. The data was analysed by student's t-test. n=1946 for P17 and n=822 for P24. (B) About 50% of P17 exhibited one nucleolus and the remainder had multiple nucleoli per nucleus. However, the proportion of cells exhibiting one nucleolus was increased to 75% in P24. The data suggests there was a decrease in the number of nucleolus per nucleus in P24.

Alternatively, an anti-fibrillarin antibody (ab4566, Abcam) with a goat anti mouse (Alexa Flour® 555) secondary antibody was used to stain nucleoli for an immunofluorescence assay (Figure 35A). Subsequently, nucleolar area was measured by CellProfiler (Figure 35B). Similarly to the previous outcome, nucleolar area was significantly enlarged in P24 ($p<0.001$), indicating RS caused increased nucleolar size (Figure 36). The average nucleolar area was 26.61µm^2 in P24 whereas it was 16.54µm^2 in P17. In addition, despite there being a diverse nucleolar size in RS, nucleolar area was generally not greater than 70µm^2 opposed to cells in OIS, which had nucleoli larger than 70µm^2.

(A)

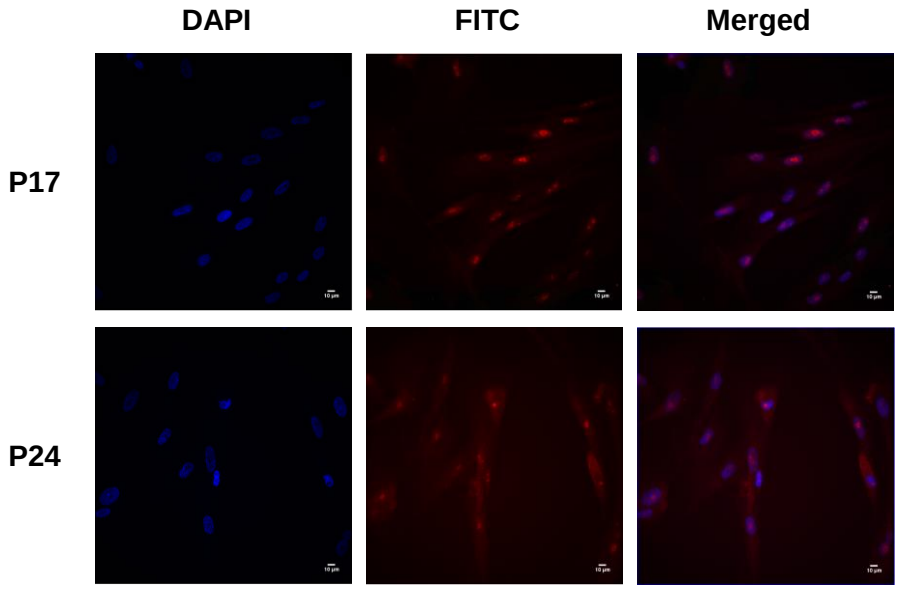

(B)

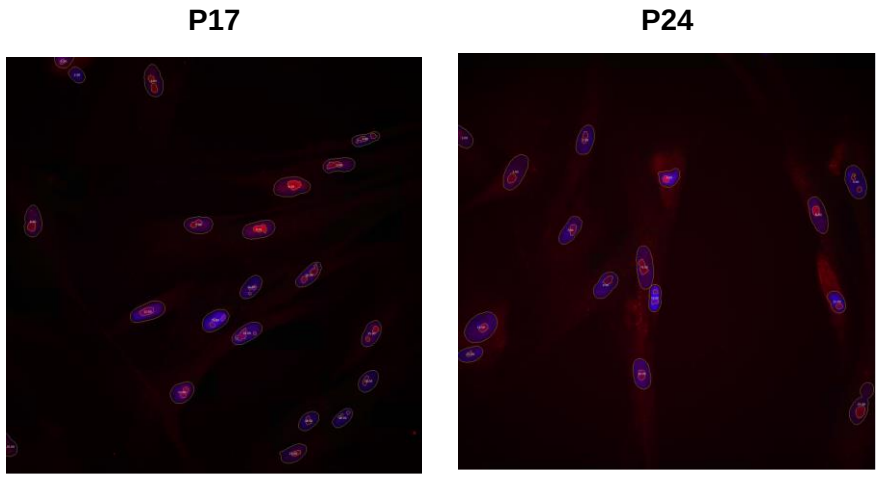

Figure 35: Immunofluorescence assay of IMR90 human fibroblasts and nucleolar area quantification by CellProfiler. (A) Anti-fibrillarin primary antibody (ab4566, Abcam) and goat anti mouse (Alexa Flour® 555) secondary antibody were used to stain the nucleoli. Following immunofluorescence, images were produced by epifluorescent microscope using x40 magnification. The scale bar is 10 µm. (B) CellProfiler was used to measure the difference in nucleolar and nuclear area between P17 and P24.

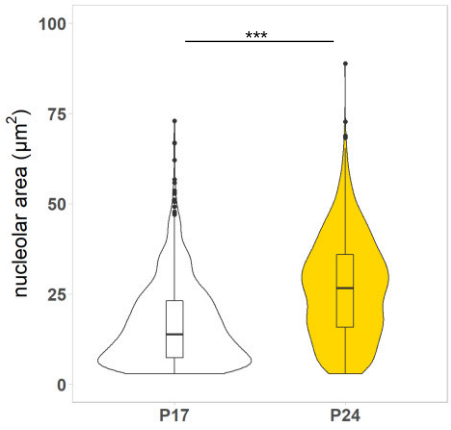

Figure 36: Nucleolar enlargement was induced by RS. Significantly increased nucleolar size was determined in P24 when compared to P17. This outcome indicated nucleolar enlargement was triggered by RS. Student's t-test was used for data analysis. n=1332 for P17 and n=1002 for P24.

Nucleolar area was examined by ImageJ using cell images from the EdU assay. Firstly, the difference in nucleolar area between early- and late-passage IMR90 was compared. As previously shown, a significant enlargement of nucleolar area was identified in P24 ($p<0.001$) (Figure 37A), substantiating the finding that RS induces nucleolar expansion. Next, EdU assay images of late-passage cells were sorted according to EdU incorporation (i.e. EdU-negative versus EdU-positive) and nucleolar area was analysed by ImageJ. As expected, nucleolar area in EdU-negative P24 was significantly greater than nucleolar area in EdU-positive P24 ($p<0.001$) (Figure 37B). This indicates replicatively senescent cells exhibited enlarged nucleoli. Yet, there was a restriction: the number of EdU-positive cells (n=11) was limited in P24 due to restricted proliferative capacity casued by long-term serial passaging. Taken together, these results suggest replicative senescence triggered nucleolar hypertrophy.

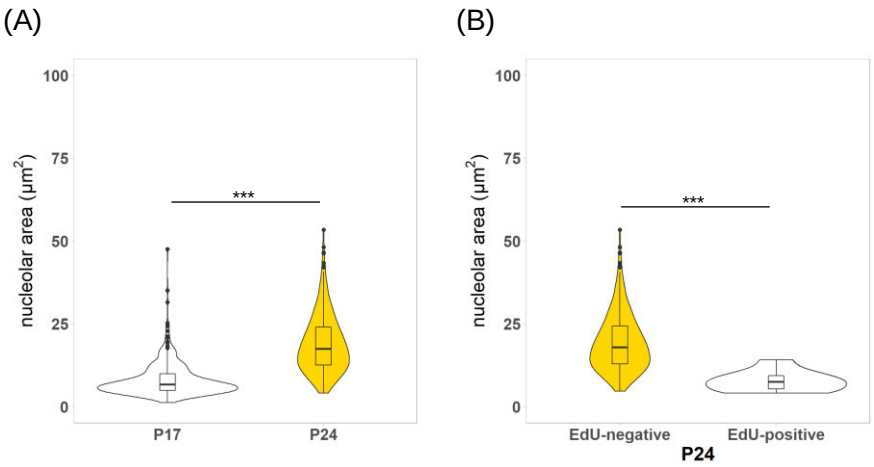

Figure 37: The comparison of nucleolar area between early and late passage cells and between EdU-positive and EdU-negative cells. (A) Significantly enlarged nucleolar area was found in P24 ($p<0.001$). The result indicates RS triggered nucleolar expansion. The mean nucleolar size was 8.08µm^2 and 18.91µm^2 in P17 and P24 respectively. The data was analysed by student's t-test. n=413 for P17 and n=331 for P24. (B) A significant increase in nucleolar size was identified in EdU-negative P24 ($p<0.001$). Student's t-test was used for analysis. n=320 and 11 for EdU-negative and –positive cells respectively.

Since nucleolar hypertrophy was found in cells that have developed OIS or RS, this raised the question of whether oncogenic and replicative stress have a similar or different impact on nucleolar dynamics. Therefore, nucleolar area was compared between cells that have entered OIS and RS. Firstly, the areas of immunofluorescently-stained nucleoli (stained with ab4566, Abcam) that were quantified by CellProfiler were compared. Surprisingly, nucleolar size was more enlarged in OIS than in RS ($p<0.001$) even though both gave rise to enlarged nucleoli (Figure 38A). More specifically, nucleolar area was nearly doubled during OIS when compared to RS (53.84µm^2 versus 26.61µm^2 on average). This result proposes OIS caused more enlarged nucleoli than RS.

Secondly, the areas of nucleoli from EdU-stained cells were quantitated by ImageJ and the results used for analysis. Likewise, OIS

triggered more severe nucleolar hypertrophy than RS ($p<0.001$), resulting in nucleoli almost twice size (33.07µm^2 versus 18.91µm^2 on average) (Figure 38B). Taken together, these results show OIS caused more substantial nucleolar enlargement than RS. Furthermore, this discovery suggests the degrees of nucleolar alterations by cellular senescence vary depending on the type of senescence inducers.

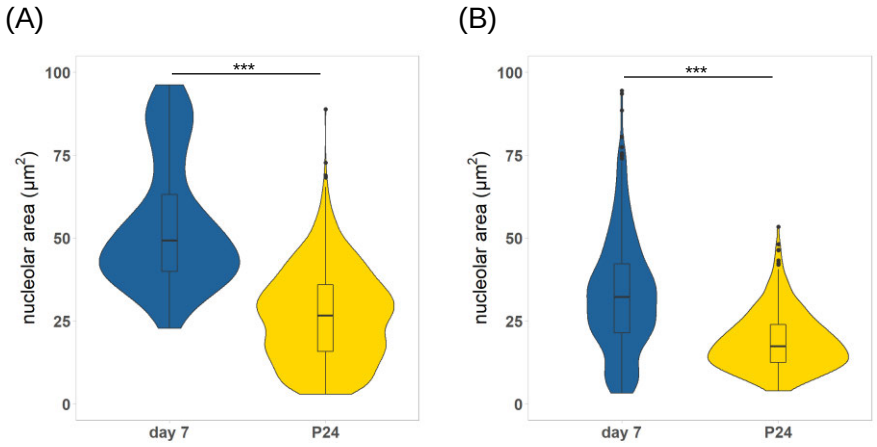

Figure 38: Nucleolar expansion was found to be more severe in OIS than RS. (A) Nucleolar size was found to be more enlarged in OIS than in RS ($p<0.001$) although increased nucleolar area was established in both types of senescence. n=50 and n=1002 for day 7 and P24 respectively. (B) More substantially enlarged nucleoli were found in cells developing OIS ($p<0.001$). n=398 and n=331 for day 7 and P24 respectively.

5.3. Investigation of intracellular changes in replicative senescence

5.3.1: Nuclear area was significantly increased, yet there was no enrichment of SAHF in replicative senescence

Following the examination of alterations of nucleolar area in RS, nuclear area was also inspected in P17 and P24 by CellProfiler. Identical to the analysis of nucleolar area, two different sets of cell images from immunofluorescence were used for nuclear area analysis.

Significantly increased nuclear size was identified in P24 ($p<0.001$) (Figure 39A and B), despite the existence of diverse nuclear area within each cell population. It follows that nuclear area was significantly enlarged by RS. One intriguing finding was that changes in nuclear area were likely a feature shared between OIS and RS, yet one that was absent from secondary senescence.

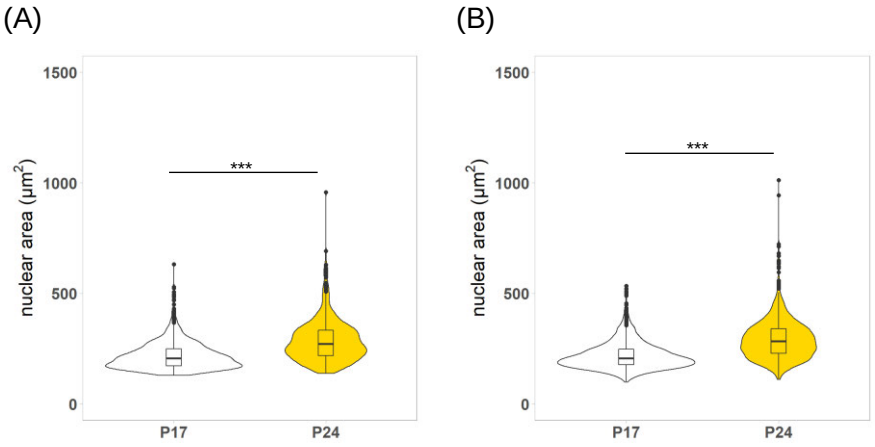

Figure 39: Significantly increased nuclear area was identified in late-passage IMR90 human fibroblasts compared to early-passage fibroblasts. (A and B) Upon the development of RS, nuclear area became significantly enlarged ($p<0.001$). This shows RS induced nuclear enlargement. Both datasets were analysed by student's t-test. (A) n=1322 and n=680 for P17 and P24 respectively. (B) n=1330 and n=1008 for P17 and P24 respectively.

In addition to the investigation of changes in nuclear area, SAHF formation in RS was inspected. Interestingly, a high proportion of SAHF-negative cells was found in late passage populations throughout the observation of cell images from the EdU and immunofluorescence assay (21 SAHF-positive cells out of 2417 cells). Such low abundance of SAHF-positive cells suggests nucleolar hypertrophy in RS is not linked with SAHF formation. Moreover, it likely implies telomere shortening, one of causes of RS, gives rise to unique nucleolar stress

compared to the nucleolar stress triggered by abnormal oncogene expression or secondary senescence inducers.

5.4. Examination of gene expression linked with alterations in nucleoli during replicative senescence

5.4.1: RPL15, RRN3, and JAZF1 were overexpressed, yet nucleolar protein genes, lamin protein genes, RPL5, RPL11, and SUN1 were repressed in replicative senescence

Finally, I investigated gene expression linked with nucleolar hypertrophy in RS using RNA-seq analysis. Like the analysis of OIS, SeqMonk software was used for quantitation, and genes that were associated with nucleolar area, structure, or morphology were utilised as probes (Table 9) to identify relevant gene expression contributing towards nucleolar alterations in RS. As a consequence of RNA-seq analysis, RPL15, RRN3, and JAZF1 were found to be upregulated while other genes such as lamin protein genes, nucleolar protein genes, RPL5, RPL11, and SUN1 were downregulated (Figure 40). The result suggests increased nucleolar size in RS was triggered by decreased expression levels of lamin genes and nucleolar protein genes along with the upregulation of RPL15, a TIF-IA transcription factor gene, and JAZF1. Not surprisingly, although enlarged nucleoli were determined to be a common feature of RS and OIS, the gene expression linked with nucleolar alterations in RS is rather different than that in OIS. In particular, the expression levels of RPL5 and RPL11 were reduced in RS, but were increased in OIS (Figure 21 and 40). JAZF1 is another gene that was found to be differently expressed in OIS and RS. Such different gene expression profiles may lead to differences between the types of senescence, for example, the disparity in nucleolar hypertrophy between OIS and RS, even though the impact of other genes excluded from this analysis must be considered. Taken together, these results indicate that the enlargement of nucleolar area in RS was likely coordinated by the upregulation of RPL15, RRN3, and JAZF1 and the downregulation of nucleolar protein genes, lamin genes, RPL5, RPL11, and SUN1.

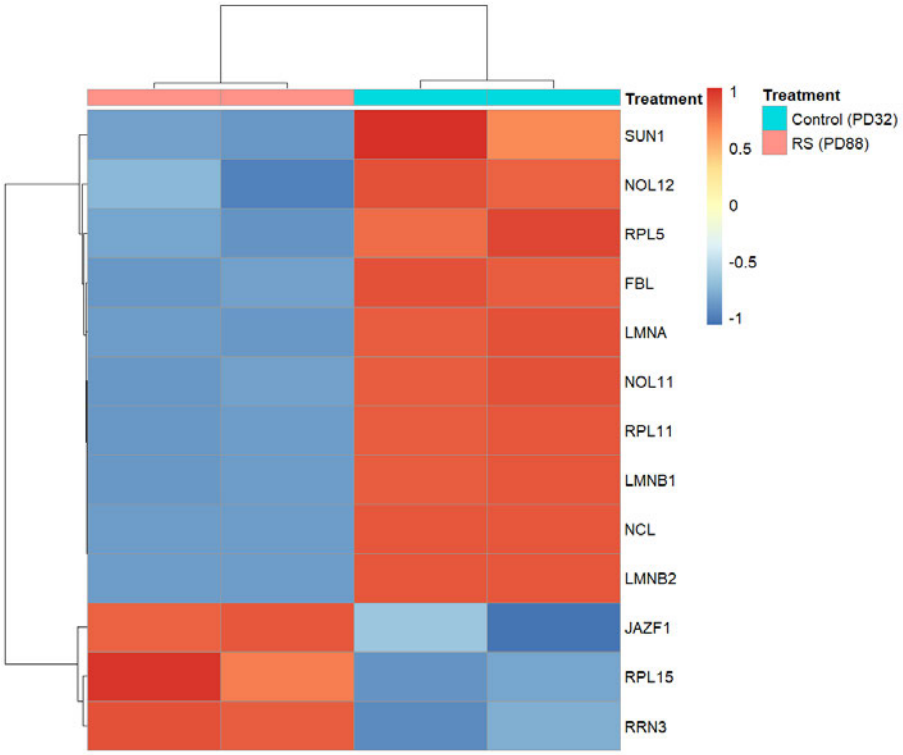

Figure 40: RNA-seq analysis of genes associated with nucleolar alterations in RS. RPL15, RRN3, and JAZF1 were overexpressed in RS. By contrast, the expression of nucleolar protein genes, lamin protein genes, RPL5, RPL11, and SUN1 was attenuated in RS. PD refers to passages.

Chapter VI

Discussion

6.1: Nucleolar expansion under nucleolar stress and diseases

In this research project, I showed the nucleolar dynamics in cellular senescence by the combination of immunofluorescence staining with subsequent automated image analysis. In earlier studies, it was proposed that senescent cells exhibit enlarged nucleoli, observed via microscopy or immunofluorescence staining (Nishimura et al., 2015; Serrano et al., 1997). Likewise, nucleolar stress induced by aspirin, viral infection, and diet restriction led to increased nucleolar size (Chen et al., 2018; Tiku et al., 2017; Wistuba et al., 1997). In support of these findings, I have demonstrated nucleolar stress induced by oncogenic or replicative stress gives rise to nucleolar hypertrophy. Moreover, the level of nucleolar expansion was significantly greater in OIS than in RS although enlarged nucleoli were a characteristic of both types of senescence. The distorted nucleolar size is currently thought to be a reflection of aberrant ribosome biogenesis. For example, enhanced rDNA transcription was identified due to the increased level of pre-rRNA generation upon the induction of OIS or RS (Nishimura et al., 2015). In agreement with this, global protein synthesis and rRNA content were substantially increased in the cells from HGPS patients and elderly donors respectively, both of which displayed enlarged nucleoli (Buchwalter and Hetzer, 2017). Such dysregulated rRNA gene transcription and ribosome production are generally coupled with characteristics of cancer cells. Indeed, most types of cancers have been reported to result in an enlarged nucleolar phenotype (MacCarty, 1936) and nucleolar size has been used as a prognostic marker for tumour identification (Derenzini et al., 2009). However, it is crucial to note that nucleolar enlargement is not a universal feature that arises due to nucleolar stress or during the pathogenesis of disease. For instance, nucleolar stress caused by bacterial infection resulted in a reduction in nucleolar size (Tiku et al., 2018). Similarly, Parkinsons's

disease (PD), a neurodegenerative disorder accompanied by the loss of dopaminergic midbrain neurons, gave rise to reduced nucleolar volume in dopaminergic neurons from patients with PD (Mann and Yates, 1982). Supporting this, decreased nucleolar volume was established in mice subjection to the partial unilateral intrastriatal 6-hydroxydopamine lesions, which model the loss of dopaminergic neurons in PD (Healy-Stoffel et al., 2013). In addition to reduced nucleolar size, nucleolar segregation – the reorganisation of nucleolar subcomponents migrating towards the nucleolar periphery along with the formation of nucleolar caps – was induced by the treatment of UV, actinomycin D, VM-26 drug (which acts as a topoisomerase II inhibitor), and chemotherapeutic drugs (Al-Baker et al., 2004; Burger et al., 2010; Chen et al., 2018; Govoni et al., 1994). It has also been shown that the reactive oxygen species, hydrogen peroxide (H_2O_2), triggers nucleolar fragmentation in C_2C_{12} myocytes (Wang et al., 2012). Nucleolar fragmentation is believed to be different from nucleolar segregation as it is characterised by the unravelling of fibrillar center induced by the inhibition of RNA polymerase II or protein kinases (David-Pfeuty, 1999; Haaf and Ward, 1996) whereas nucleolar segregation is in particular created by the perturbation of rRNA transcription (Burger et al., 2010; Chen et al., 2018; Yang et al., 2018). Taken together, these findings suggest nucleolar expansion is one of many nucleolar alterations found in nucleolar stress and the development of diseases. A variety of stressors can give rise to diverse nucleolar phenotypes such as decreased nucleolar size, nucleolar segregation, and nucleolar fragmentation.

The increase in nucleolar size during OIS and RS is thought to be related with the decreased number of nucleolus per nucleus. Indeed, a reduced number of nucleolus per nucleus was found under nucleolar stress caused by OIS and RS, normative aging, and HGPS (Buchwalter and Hetzer, 2017; Nishimura et al., 2015; Pinho et al., 2019). In parallel with these findings, I identified a decrease in the number of nucleolus per nucleus when RS was established. However, there is no direct evidence showing small nucleoli merge together to form a greater nucleolus or nucleoli, thereby this theory remains to be

evaluated. For instance, time-lapse fluorescence microscopy with stable nucleolar markers can be utilised to investigate this hypothesis. Moreover, additional research needs to be performed to understand the nucleolar size gap between OIS and RS, and what it means biologically. One possible cause of the different nucleolar phenotypes under nucleolar stress could be Alu element-containing RNAs. A recent study showed that RNA polymerase II transcripts originating from intronic Alu elements (aluRNAs) play an essential role in nucleolar integrity (Caudron-Herger et al., 2015). While the disruption of aluRNAs or RNA polymerase II resulted in nucleolar dispersion and impaired rRNA gene transcription, the overexpression of aluRNAs led to enlarged nucleoli and increased pre-rRNA levels (Caudron-Herger et al., 2015). Furthermore, nucleolar proteins including fibrillarin, nucleolin, and nucleophosmin were found to interact with aluRNAs and the authors proposed aluRNAs may serve as a 'glue' that coordinates the assembly or disassembly of nucleolar formations (Caudron-Herger et al., 2015). Nevertheless, the question remains what mechanisms govern the differentiation of nucleolar integrity under the distinct conditions of nucleolar stress and diseases.

The nucleolar dynamics in cells that have developed secondary senescence are highlighted for the first time by this research project. I found secondary senescence did not trigger nucleolar expansion, which was surprisingly different from OIS and RS, which exhibited nucleolar hypertrophy. The development of secondary senescence in mVenus:EV cells relied on cell-cell communication including SASP and Notch signalling (Hoare et al., 2016; Teo et al., 2019) during co-culture with OIS-induced ER:Ras IMR90 for up to seven days. To further confirm the effect of secondary senescence on nucleolar size, more experiments need to be repeated. Furthermore, it may be worthwhile using a long term co-culture system, for example, 14 days of co-culture with ER:Ras IMR90, to identify and understand the impact on nucleolar size of secondary senescence as seven days of co-culture may not be sufficient to observe the changes to nucleolar dynamics arising in secondary senescence.

6.2. Nucleolar expansion alongside alterations in nuclear size and SAHF formation

I determined different senescence inducers caused nucleolar stress that accompanied distinct intracellular changes along with enlarged nucleolar area. For instance, OIS-induced and replicatively senescent cells exhibited increased nuclear size, but cells established in secondary senescence did not. The distorted nuclear area is believed to be partly due to disrupted nuclear components such as lamins and SUN proteins, which localise to the nuclear envelope and whose primary function is to maintain nuclear architecture (Gupta and Sengupta, 2017; Matsumoto et al., 2016). Indeed, the depletion of lamin A/C, SUN1, and SUN2 genes resulted in changes to nuclear shape (Matsumoto et al., 2016). Additionally, cells derived from HGPS patients expressed progerin which incorporates into the nuclear scaffold, leading to disruption of the nuclear phenotype (Goldman et al., 2004). Supporting these findings, I also identified the downregulation of lamin genes including LMNA, LMNB1, and LMNB2 in both OIS and RS through RNA-seq analysis. In addition, SUN1 was also found to be repressed in RS. Taken together, it most likely suggests the gene expression of nuclear components was altered during OIS and RS, which was reflected in increased nuclear size.

Although OIS and RS share the features of enlarged nucleolar and nuclear area, SAHF were, in particular, enriched in OIS but were not in RS and secondary senescence. This result is in parallel with previous findings: SAHF formation was exclusively identified in OIS, yet not in secondary senescence or RS (Kosar et al., 2011; Parry et al., 2018; Teo et al., 2019). Even though causes of such different chromatin features are not entirely clear, a number of researches have shed light on them in different types of cellular senescence. One aspect is shifted senescence-associated heterochromatin domain (SAHDs) interactions in OIS. Recently multi-omics, together with imaging approaches in OIS- and RS-induced human fibroblasts, revealed the implication of SAHDs in SAHF formation (Sati et al., 2020). Cells that had developed OIS showed the loss of intra-SAHD interactions and the gain of inter-SAHD

interactions in *trans*, while RS revealed no significant alterations in inter- or intra-SAHD interactions (Sati et al., 2020). Moreover, it was shown that DNA methyltransferase 1 (DNMT1) was a key protein in the development of SAHF because the depletion of DNMT1 resulted in the prevention of SAHF formation and DNMT1-depleted OIS cells displayed a 3D genome conformation similar to the one from RS-induced cells (Sati et al., 2020). Another contributor towards SAHF formation is Notch signalling which was shown to be an alternative mechanism of propagating secondary senescence in a juxtacrine manner (Teo et al., 2019). Notch-induced senescence (NIS) was shown to have low levels of SHAF formation and to have distinct gene expression profiles compared to OIS (Teo et al., 2019). Another study evidenced that Notch signalling resulted in a chromatin smoothening effect and the inhibition of SAHF formation by repressing High-Mobility Group A (HMGA) proteins (Parry et al., 2018) that were previously found to be an activator of SAHF formation (Narita et al., 2006). In summary, prevalent SAHF-negative features identified in RS and secondary senescence are thought to be produced by differential SAHDs interaction and Notch signalling to a limited extent.

In addition to this, I propose SAHF formation is likely linked with enlarged nucleoli in OIS as SAHF-positive cells seemed to exhibit significantly enlarged nucleoli than SHAF-negative cells. This is the first evidence of this correlation, yet little else is known. Despite different SAHD interaction, OIS and RS showed nucleolar enlargement, and it is therefore feasible to hypothesise SAHDs may be independent of alterations in nucleolar size. It will be interesting to investigate the effect of DNMT1, Notch signalling, and HMGA on nucleolar hypertrophy to better understand the association between SAHF formation and nucleolar expansion.

6.3. Genes expressed alongside alterations in nucleolar area

RNA-seq analysis revealed changed gene expression linked to nucleolar hypertrophy in OIS and RS. It was previously shown that the knockdown of RPL15 and TIF-IA caused the disruption of nucleolar

integrity, ribosome biogenesis, and the cell cycle (Chen et al., 2018; Dong et al., 2019; Hayashi et al., 2018). Similarly, other studies reported the gene silencing of nucleolar protein-encoding genes including FBL, NCL, UBF, NOL11, and NOL12 resulted in alterations to nucleolar size or morphology and disrupted ribosome biogenesis (Hayashi et al., 2018; Pinho et al., 2019; Tiku et al., 2017; Ugrinova et al., 2007). I found OIS and RS share overexpression of RPL15 and TIF-IA gene and repression of nucleolar protein-encoding genes including FBL, NCL, NOL11, and NOL12. This altered gene expression likely resulted in the impaired protein functions in the gene products. Functions such as the initiation of rDNA transcription, the production of ribosomal proteins, and the processing of pre-rRNAs and rRNAs, all of which eventually influenced ribosome generation. Accordingly, the compromised ribosome biogenesis was likely reflected in the changed nucleolar size in OIS and RS. Intriguingly, RPL5 and RPL11 were differentially expressed: they were upregulated in OIS while supressed in RS. JAZF1 was repressed in OIS, yet overexpressed in RS. The implication of such different gene expression under OIS and RS is largely unknown, but one speculation is that OIS and RS have a different molecular axis that controls the MDM2-p53 pathway. RPL5 and RPL11 together with 5S rRNA were found to form a ribonucleoprotein complex that mediates p53 stabilisation and activation (Donati et al., 2013). The downregulation of RPL5 and RPL11 in RS likely suggests nucleolar stress caused by RS requires the involvement of other molecular pathways in the regulation of p53 activation.

Here, the effectiveness of the RNA-seq analysis is limited because RNA-seq was performed using OIS- and RS-induced cells without the separation of cells according to nucleolar size. Therefore, the RNA-seq data does not fully represent gene expression in relation to nucleolar hypertrophy. For future research to obtain better insights into the genes that contribute to nucleolar expansion in OIS and RS, I suggest dividing cells based on nucleolar size through immunofluorescence staining with nucleolar markers and subsequent sorting via fluorescence-associated cell sorter (FACS) and VyCap Puncher, then performing

single cell RNA-seq. This will likely provide an idea of genes playing a key role in alterations in nucleolar size. Furthermore, these reults could be utilised for comparison with the known transcriptional signatures of ageing since nucleolar size seems to be linked with longevity.

In conclusion, I have elucidated the nucleolar dynamics in OIS, secondary senescence, and RS. In addition, other intracellular changes including enlarged nuclear size and SAHF formation in parallel with alterations in nucleolar size have been revealed under different types of senescence. Lastly, RNA-seq analysis revealed distinct gene expression profiles in OIS and RS. The results I obtained support previous findings and there are a few discoveries that have been first described in this project. For example, secondary senescence does not cause nucleolar expansion. Secondly, OIS gives rise to more significantly enlarged nucleoli than RS. Lastly, nucleolar hypertrophy seems to be linked with SAHF formation in OIS. This research opens the door for further investigation to advance our understanding of the nucleolar stress caused by cellular senescence.

References

Acosta, J.C., O'Loghlen, A., Banito, A., Guijarro, M.V., Augert, A., Raguz, S., Fumagalli, M., Costa, M.D., Brown, C., Popov, N., Takatsu, Y., Melamed, J., d'Adda di Fagagna, F., Bernard, D., Hernando, E., Gil, J. (2008). Chemokine Signaling via the CXCR2 Receptor Reinforces Senescence. Cell *133*, 1006-1018.

Ahmad, Y., Boisvert, F.-M., Gregor, P., Cobley, A., Lamond, A.I. (2009). NOPdb: Nucleolar Proteome Database—2008 update. Nucleic Acids Res. *37*, D181-D184.

Al-Baker, E.A., Boyle, J., Harry, R., Kill, I.R. (2004). A p53-independent pathway regulates nucleolar segregation and antigen translocation in response to DNA damage induced by UV irradiation. Exp. Cell. Res. *292*, 179-186.

Anderson, J.S., Lam, Y.W., Leung, A.K.L., Ong, S.-E., Lyon, C.E., Lamond, A.I., Mann, M. (2005). Nucleolar proteome dynamics. Nature *433*, 77-83.

Anderson, J.S., Lyon, C.E., Fox, A.H., Leung, A.K.L., Lam, Y.W., Steen, H., Mann, M., Lamond, A.I. (2002). Directed Proteomic Analysis of the Human Nucleolus. Curr. Biol. *8*, 1-11.

Bartkova, J., Rezaei, N., Liontos, M., Karakaidos, P., Kletsas, D., Issaeva, N., Vassiliou, L.-V.F., Kolettas, E., Niforou, K., Zoumpourlis, V.C., Takaoka, M., Nakagawa, H., Tort, F., Fugger, K., Johansson, F., Sehested, M., Andersen, C.L., Dyrskjot, L., Ørntoft, T., Lukas, J., Kittas, C., Helleday, T., Halazonetis, T.D., Bartek, J., Gorgoulis, V.G. (2006). Oncogene-induced senescence is part of the tumorigenesis barrier imposed by DNA damage checkpoints. Nature *444*, 633-637.

Bodnar, A.G., Ouellette, M., Frolkis, M., Holt, S.E., Chiu, C.-P., Morin, G.B., Harley, C.B., Shay, J.W., Lichtsteiner, S., Wright, W.E. (1998). Extension of Life-Span by Introduction of Telomerase into Normal Human Cells. Science *279*, 349-352.

Boisvert, F.M., Lam, Y.W., Lamont, D., Lamond, A.I. (2010). A Quantitative Proteomics Analysis of Subcellular Proteome Localization and Changes Induced by DNA Damage. Mol. Cell. Proteomics *9*, 457-470.

Boisvert, F.M., van Koningsbruggen, S., Navascués, J., Lamond, A.I. (2007). The multifunctional nucleolus. Nat. Rev. Mol. Cell. Biol. *8*, 574-585.

Birnstiel, M.L., Wallace, H., Sirlin, J.L., Fischberg, M. (1966). Localization of the Ribosomal DNA Complements in the Nucleolar Organizer Region of *Xenopus laevis*. Natl. Cancer Inst. Monogr. *23*, 431-447.

Buchwalter, A. and Hetzer, M.W. (2017). Nucleolar expansion and elevated protein translation in premature aging. Nat. Commun. *8*, 328.

Burger, K., Mühl, B., Harasim, T., Rohrmoser, M., Malamoussi, A., Orban, M., Kellner, M., Gruber-Eber, A., Kremmer, E., Hölzel, M., Eick, D. (2010). Chemotherapeutic Drugs Inhibit Ribosome Biogenesis at Various Levels. J. Biol. Chem. *285*, 12416-12425.

Campisi, J. and d'Adda di Fagagna, F. (2007). Cellular senescence: when bad things happen to good cells. Nat. Rev. Mol. Cell. Biol. *8*, 729-740.

Caudron-Herger, M., Pankert, T., Seiler, J., Németh, A., Voit, R., Grummt, I., Rippe, K. (2015). Alu element-containing RNAs maintain nucleolar structure and function. EMBO J. *34*, 2758-2774.

Chan, P.-K., Aldrich, M.B., Yung, B.Y.-M. (1987). Nucleolar Protein B23 Translocation after Doxorubicin Treatment in Murine Tumor Cells. Cancer Res. *47*, 3798-3801.

Chandra, T., Kirschner, K., Thuret, J.-Y., Pope, B.D., Ryba, T., Newman, S., Ahmed, K., Samarajiwa, S.A., Salama, R., Carroll, T., Stark, R., Janky, R., Narita, M., Xue, L., Chicas, A., Nũnez, S., Janknecht, R., Hayashi-Takanaka, Y., Wilson, M.D., Marshall, A., Odom, D.T., Babu, M.M., Bazett-Jones, D.P., Tavaré, S., Edwards, P.A.W., Lowe, S.W., Kimura, H., Gilbert, D.M., Narita, M. (2012). Independence of Repressive Histone Marks and Chromatin Compaction during Senescent Heterochromatic Layer Formation. Mol. Cell *47*, 203-214.

Chen, J., Lobb, I.T., Morin, P., Novo, S.M., Simpson, J., Kennerknecht, K., von Kriegsheim, A., Batchelor, E.E., Oakley, F., Stark, L.A. (2018). Identification of a novel TIF-IA-NF-κB nucleolar stress response pathway. Nucleic Acids Res. *46*, 6188-6205.

d'Adda di Fagagna, F. Reaper, P.M., Clay-Farrace, L., Fiegler, H., Carr, P., von Zglinicki, T., Saretzki, G., Carter, N.P., Jackson, S.P. (2003). A DNA damage checkpoint response in telomere-initiated senescence. Nature *426*, 194-198.

d'Adda di Fagagna, F. (2008). Living on a break: cellular senescence as a DNA-damage response. Nat. Rev. Cancer *8*, 512-522.

Dai, M.-S. and Lu, H. (2004). Inhibition of MDM2-mediated p53 ubiquitination and degradation by ribosomal protein L5. J. Biol. Chem. *279*, 44475-44482.

David-Pfeuty, T. (1999). Potent inhibitors of cyclin-dependent kinase 2 induce nuclear accumulation of wild-type p53 and nucleolar fragmentation in human untransformed and tumor-derived cells. Oncogene *18*, 7409-7422.

Denchi, E.L. and de Lange, T. (2007). Protection of telomeres through independent control of ATM and ATR by TRF2 and POT1. Nature *448*, 1068-1071.

Derenzini, M., Montanaro, L., Treré, D. (2009). What the nucleolus says to a tumour pathologist. Histopathology *54*, 753-762.

Di Micco, R., Fumagalli, M., Cicalese, A., Piccinin, S., Gasparini, P., Luise, C., Schurra, C., Garre', M., Nuciforo, P.G., Bensimon, A., Maestro, R., Pelicci, P.G., d'Adda di Fagagna, F. (2006). Oncogene-induced senescence is a DNA damage response triggered by DNA hyper-replication. Nature *444*, 638-642.

Dimri, G.P., Lee, X., Basile, G., Acosta, M., Scott, G., Roskelley, C., Medrano, E.E., Linskens, M., Rubelj, I., Pereira-Smith, O. (1995). A biomarker that identifies senescent human cells in culture and in aging skin in vivo. Proc. Natl. Acad. Sci. U. S. A. *92*, 9363-9367.

Donati, G., Peddigari, S., Mercer, C.A., Thomas, G. (2013). 5S Ribosomal RNA Is an Essential Component of a Nascent Ribosomal Precursor Complex that Regulates the Hdm2-p53 Checkpoint. Cell Rep. *4*, 87-98.

Dong, Z., Jiang, H., Liang, S., Wang, Y., Jiang, W., Zhu, C. (2019). Ribosomal Protein L15 is involved in Colon Carcinogenesis. Int. J. Med. Sci. *16*, 1132-1141.

Freed, E.F., Prieto, J.-L., McCann, K.L., McStay, B., Baserga, S.J. (2012). NOL11, Implicated in the Pathogenesis of North American Indian Childhood Cirrhosis, Is Required for Pre-rRNA Transcription and Processing. PLoS Genet. *8*, e1002892.

Goldman, R.D., Shumaker, D.K., Erdos, M.R., Eriksson, M., Goldman, A.E., Gordon, L.B., Gruenbaum, Y., Khuon, S., Mendez, M., Varga, R., Collins, F.S. (2004). Accumulation of mutant lamin A causes progressive changes in nuclear architecture in Hutchinson-Gilford progeria syndrome. Proc. Natl. Acad. Sci. U. S. A. *101*, 8963-8968.

Govoni, M., Farabegoli, F., Pession, A., Novello, F. (1994). Inhibition of Topoisomerase II Activity and Its Effect on Nucleolar Structure and Function. Exp. Cell Res. *211*, 36-41.

Gupta, A.S. and Sengupta, K. (2017). Lamin B2 Modulates Nucleolar Morphology, Dynamics, and Function. Mol. Cell. Biol. *37*, e00274-17.

Haaf, T. and Ward, D.C. (1996). Inhibition of RNA Polymerase II Transcription Causes Chromatin Decondensation, Loss of Nucleolar Structure, and Dispersion of Chromosomal Domains. Exp. Cell Res. *224*, 163-173.

Harley, C., Futcher, A., Greider, C. (1990). Telomeres shorten during ageing of human fibroblasts. Nature *345*, 458-460.

Hayashi, Y., Fujimura, A., Kato, K., Udagawa, R., Hirota, T., Kimura, K. (2018). Nucleolar integrity during interphase supports faithful Cdk1 activation and mitotic entry. Sci. Adv. *4*, eaap7777.

Hayflick, L. (1965). The limited *in vitro* lifetime of human diploid cell strains. Exp. Cell Res. *37*, 614-636.

Hayflick, L. and Moorhead, P.S. (1961). The serial cultivation of human diploid cell strains. Exp. Cell Res. *25*, 585-621.

Healy-Stoffel, M., Ahmad, S.O., Stanford, J.A., Levant, B. (2013). Altered nucleolar morphology in substantia nigra dopamine neurons following 6-hydroxydopamine lesion in rats. Neurosci. Lett. *546*, 26-30.

Hein, N., Hannan, K.M., George, A.J., Sanij, E., Hannan, R.D. (2013). The nucleolus: an emerging target for cancer therapy. Trends. Mol. Med. *19*, 643-654.

Henderson, A.S., Warburton, D., Atwood, K.C. (1972). Location of Ribosomal DNA in the Human Chromosome Complement. Proc. Natl. Acad. Sci. U. S. A. *69*, 3394-3398.

Henras, A.K., Plisson-Chastang, C., O'Donohue, M.-F., Chakraborty, A., Gleizes, P.-E. (2015). An overview of pre-ribosomal RNA processing in eukaryotes. Wiley. Interdiscip. Rev. RNA. *6*, 225-242.

Herbig, U., Jobling, W.A., Chen, B.P.C., Chen, D.J., Sedivy, J.M. (2004). Telomere Shortening Triggers Senescence of Human Cells through a Pathway Involving ATM, p53, and p21(CIP1), but Not p16(INK4a). Mol. Cell *14*, 501-513.

Hoare, M., Ito, Y., Kang, T.-W., Weekes, M.P., Matheson, N.J., Patten, D.A., Shetty, S., Parry, A.J., Menon, S., Salama, R., Antrobus, R., Tomimatsu, K., Howat, W., Lehner, P.J., Zender, L., Narita, M. (2016). NOTCH1 mediates a switch between two distinct secretomes during senescence. Nat. Cell Biol. *18*, 979-992.

Jones, C.J., Kipling, D., Morris, M., Hepburn, P., Skinner, J., Bounacer, A., Wyllie, F.S., Ivan, M., Bartek, J., Wynford-Thomas, D., Bond, J.A. (2000). Evidence for a Telomere-Independent "Clock" Limiting *RAS* Oncongene-Driven Proliferation of Human Thyroid Epithelial Cells. Mol. Cell. Biol. *20*, 5690-5699.

Karlseder, J., Hoke, K., Mirzoeva, O.K., Bakkenist, C., Kasten, M.B., Petrini, J.H.J., de Lange, T. (2004). The Telomeric Protein TRF2 Binds the ATM Kinase and Can Inhibit the ATM-Dependent DNA Damage Response. PLoS Biol. *2*, e240.

Kobiita, A., Godbersen, S., Araldi, E., Ghoshdastider, U., Schmid, M.W., Spinas, G., Moch, H., Stoffel, M. (2020). The Diabetes Gene JAZF1 Is Essential for the Homeostatic Control of Ribosome Biogenesis and Function in Metabolic Stress. Cell Rep. *32*, 107846.

Kosar, M., Bartkova, J., Hubackova, S., Hodny, Z., Lukas, J., Bartek, J. (2011). Senescence-associated heterochromatin foci are dispensable for cellular senescence, occur in a cell type- and insult-dependent manner and follow expression of p16(ink4a). Cell Cycle *10*, 457-468.

Kuilman, T., Michaloglou, C., Mooi, W.J., Peeper, D.S. (2010). The essence of senescence. Genes Dev. *24*, 2463-2479.

Kumazawa, T., Nishimura, K., Katagiri, N., Hashimoto, S., Hayashi, Y., Kimura, K. (2015). Gradual reduction in rRNA transcription triggers p53 acetylation and apoptosis via MYBBP1A. Sci. Rep. *5*, 10854.

Kurki, S., Peltonen, K., Latonen, L., Kiviharju, T.M., Ojala, P.M., Meek, D., Laiho, M. (2004). Nucleolar protein NPM interacts with HDM2 and protects tumor suppressor protein p53 from HDM2-mediated degradation. Cancer Cell. *5*, 465-475.

Lee, J.H., Lee, Y.S., Jeong, S.A., Khadka, P., Roth, J., Chung, I.K. (2014). Catalytically active telomerase holoenzyme is assembled in the dense fibrillar component of the nucleolus during S phase. Histochem. Cell. Biol. *141*, 137-152.

Lee, S., Kim, J.-Y., Kim, Y.-J., Seok, K.-O., Kim, J.-H., Chang, Y.-J., Kang, H.-Y., Park, J.-H. (2012). Nucleolar protein GLTSCR2 stabilizes p53 in response to ribosomal stresses. Cell Death Differ. *19*, 1613-1622.

Li, M. and Gu, W. (2011). A Critical Role for Noncoding 5S rRNA in Regulating Mdmx Stability. Mol. Cell *43*, 1023-1032.

Lin, A.W., Barradas, M., Stone, J.C., van Aelst, L., Serrano, M., Lowe, S.W. (1998). Premature senescence involving p53 and p16 is activated in response to constitutive MEK/MAPK mitogenic signaling. Genes Dev. *12*, 3008-3019.

MacCarty, W.C. (1936). The Value of the Macronucleolus in the Cancer Problem. American Association for Cancer Research *26*, 529-532.

Mann, D.M. and Yates, P.O. (1982). Pathogenesis of Parkinson's disease. Arch. Neurol. *39*, 545-549.

Martin, C., Chen, S., Maya-Mendoza, A., Lovric, J., Sims, P.F.G., Jackson, D.A. (2009). Lamin B1 maintains the functional plasticity of nucleoli. J. Cell Sci. *122*, 1551-1562.

Matsumoto, A., Sakamoto, C., Matsumori, H., Katahira, J., Yasuda, Y., Yoshidome, K., Tsujimoto, M., Goldberg, I.G., Matsuura, N., Nakao, M., Saitoh, N., Hieda, M. (2016). Loss of the integral nuclear envelope protein SUN1 induces alteration of nucleoli. Nucleus *7*, 68-83.

McClintock, B. (1934). The relation of a particular chromosomal element to the development of the nucleoli in Zea mays. Z. Zellforsch. *21*, 294-326.

Narita, M., Narita, M., Krizhanovsky, V., Nuñez, S., Chicas, A., Hearn, S.A., Myers, M.P., Lowe, S.W. (2006). A Novel Role for High-Mobility Group A Proteins in Cellular Senescence and Heterochromatin Formation. Cell *126*, 503-514.

Narita, M., Nuñez, S., Heard, E., Narita, M., Lin, A.W., Hearn, S.A., Spector, D.L., Hannon, G.J., Lowe, S.W. (2003). Rb-Mediated Heterochromatin Formation and Silencing of E2F Target Genes during Cellular Senescence. Cell *113*, 703-716.

Nicolas, E., Parisot, P., Pinto-Monteiro, C., de Walque, R., Vleeschouwer, C.D., Lafontaine, D.L.J. (2016). Involvement of human ribosomal proteins in nucleolar structure and p53-dependent nucleolar stress. Nat. Commun. *7*, 11390.

Nishimura, K., Kumazawa, T., Kuroda, T., Katagiri, N., Tsuchiya, M., Goto, N., Furumai, R., Murayama, A., Yanagisawa, J., Kimura, K. (2015). Perturbation of Ribosome Biogenesis Drives Cells into Senescence through 5S RNP-Mediated p53 Activation. Cell Rep. *10*, 1310-1323.

Palm, W. and de Lange, T. (2008). How Shelterin Protects Mammalian Telomeres. Annu. Rev. Genet. *42*, 301-334.

Parry, A.J., Hoare, M., Bihary, D., Hänsel-Hertsch, R., Smith, S., Tomimatsu, K., Mannion, E., Smith, A., D'Santos, P., Russell, I.A., Balasubramanian, S., Kimura, H., Samarajiwa, S.A., Narita, M. (2018). NOTCH-mediated non-cell autonomous regulation of chromatin structure during senescence. Nat. Commun. *9*, 1840.

Pérez-Mancera, P.A., Young, A.R.J., Narita, M. (2014). Inside and out: the activities of senescence in cancer. Nat. Rev. Cancer *14*, 547-558.

Pinho, M., Macedo, J.C., Logarinho, E., Pereira, P.S. (2019). NOL12 Repression Induces Nucleolar Stress-Driven Cellular Senescence and Is Associated with Normative Aging. Mol. Cell. Biol. *39*, e00099-19.

Rai, T.S., Cole, J.J., Nelson, D.M., Dikovskaya, D., Faller, W.J., Vizioli, M.G., Hewitt, R.N., Anannya, O., McBryan, T., Manohara, I., van Tuyn, J., Morrice, N., Pchelintsev, N.A., Ivanov, A., Brock, C., Drotar, M.E., Nixon, C., Clark, W., Sansom, O.J., Anderson, K.I., King, A., Blyth, K., Adams, P.D. (2014). HIRA orchestrates a dynamic chromatin landscape in senescence and is required for suppression of neoplasia. Genes Dev. *28*, 2712-2725.

Ritossa, F.M., and Spiegelman, S. (1965). Localization of DNA Complementary to Ribosomal RNA in the Nucleolus Organizer Region of Drosophila melanogaster. Proc. Natl. Acad. Sci. U. S. A. *53*, 737-745.

Rubbi, C.P. and Milner, J. (2003). Disruption of the nucleolus mediates stabilization of p53 in response to DNA damage and other stresses. EMBO J. *22*, 6068-6077.

Sati, S., Bonev, B., Szabo, Q., Jost, D., Bensadoun, P., Serra, F., Loubiere, V., Papadopoulos, G.L., Rivera-Mulia, J.-C., Fritsch, L., Bouret, P., Castillo, D., Gelpi, J.L.I., Orozco, M., Vaillant, C., Pellestor, F., Bantignies, F., Marti-Renom, M.A., Gilbert, D.M., Lemaitre, J.-M., Cavalli, G. 4D Genome Rewiring during Oncogene-Induced and Replicative Senescence. (2020). Mol. Cell *78*, 522-538.e9.

Serrano, M., Lin, A.W., McCurrach, M.E., Beach, D., Lowe, S.W. (1997). Oncogenic *ras* Provokes Premature Cell Senescence Associated with Accumulation of p53 and $p16^{INK4a}$. Cell *88*, 593-602.

Sinclair, D.A., Mills, K., Guarente, L. (1997). Accelerated Aging and Nucleolar Fragmentation in Yeast sgs1 Mutants. Science *277*, 1313-1316.

Teo, Y.V., Rattanavirotkul, N., Olova, N., Salzano, A., Quintanilla, A., Tarrats, N., Kiourtis, C., Müller, M., Green, A.R., Adams, P.D., Acosta, J.-C., Bird, T.G., Kirschner, K., Neretti, N., Chandra, T. (2019). Notch

Signaling Mediates Secondary Senescence. Cell Rep. *27*, 997-1007.e5.

Tiku, V., Jain, C., Raz, Y., Nakamura, S., Heestand, B., Liu, W., Späth, M., Suchiman, H.E.D., Müller, R.-U., Slagboom, P.E., Patridge, L., Antebi, A. (2017). Small nucleoli are a cellular hallmark of longevity. Nat. Commun. *8*, 16083.

Tiku, V., Kew, C., Mehrotra, P., Ganesan, R., Robinson, N., Antebi, A. (2018). Nucleolar fibrillarin is an evolutionarily conserved regulator of bacterial pathogen resistance. Nat. Commun. *9*, 3607.

Ugrinova, I., Monier, K., Ivaldi, C., Thiry, M., Storck, S., Mongelard, F., Bouvet, P. (2007). Inactivation of nucleolin leads to nucleolar disruption, cell cycle arrest and defects in centrosome duplication. BMC Molecular Biol. *8*, 66.

Wang, K., Deng, G., Chen, G., Liu, M., Yi, Y., Yang, T., McMillan, D.R., Xiao, X. (2012). Heat shock protein 70 inhibits hydrogen peroxide-induced nucleolar fragmentation via suppressing cleavage and down-regulation of nucleolin. Cell Stress Chaperones. *17*, 121-130.

Wistuba, A., Kern, A., Weger, S., Grimm, D., Kleinschmidt, J.A. (1997). Subcellular Compartmentalization of Adeno-Associated Virus Type 2 Assembly. J. Virol. *71*, 1341-1352.

Yang, K., Yang, J., Yi, J. (2018). Nucleolar Stress: hallmarks, sensing mechanism and diseases. Cell Stress. *2*, 125-140.

Yuan, X., Zhou, Y., Casanova, E., Chai, M., Kiss, E., Gröne, H.-J., Schütz, G., Grummt, I. (2005). Genetic Inactivation of the Transcription Factor TIF-IA Leads to Nucleolar Disruption, Cell Cycle Arrest, and p53-Mediated Apoptosis. Mol. Cell *19*, 77-87.

Zhang, Y., Wolf, G.W., Bhat, K., Jin, A., Allio, T., Burkhart, W.A., Xiong, Y. (2003). Ribosomal Protein L11 Negatively Regulates Oncoprotein MDM2 and Mediates a p53-Dependent Ribosomal-Stress Checkpoint Pathway. Mol. Cell. Biol. *23*, 8902-8912.

Zhang, R., Chen, W., Adams, P.D. (2007). Molecular Dissection of Formation of Senescence-Associated Heterochromatin Foci. Mol. Cell. Biol. *27*, 2343-2358.

Zhu, J., Woods, D., McMahon, M., Bishop, J.M. (1998). Senescence of human fibroblasts induced by oncogenic Raf. Genes Dev. *12*, 2997-3007.